IEEE Access
Multidisciplinary | Rapid Review | Open Access Journal

Received August 19, 2016, accepted August 29, 2016, date of publication September 13, 2016, date of current version October 6, 2016.

Digital Object Identifier 10.1109/ACCESS.2016.2608621

Metal Artifact Reduction in CT: Where Are We After Four Decades?

LARS GJESTEBY[1], BRUNO DE MAN[2], YANNAN JIN[2], HARALD PAGANETTI[3], JOOST VERBURG[3], DROSOULA GIANTSOUDI[3], AND GE WANG[1] (Fellow, IEEE)

[1]Biomedical Imaging Center, Department of Biomedical Engineering, Rensselaer Polytechnic Institute, Troy, NY 12180, USA
[2]Image Reconstruction Laboratory, General Electric Global Research Center, Niskayuna, NY 12309, USA
[3]Department of Radiation Oncology, Harvard Medical School, Massachusetts General Hospital, Boston, MA 02114, USA

Corresponding authors: B. De Man (deman@ge.com) and G. Wang (ge-wang@ieee.org)

ABSTRACT Methods to overcome metal artifacts in computed tomography (CT) images have been researched and developed for nearly 40 years. When X-rays pass through a metal object, depending on its size and density, different physical effects will negatively affect the measurements, most notably beam hardening, scatter, noise, and the non-linear partial volume effect. These phenomena severely degrade image quality and hinder the diagnostic power and treatment outcomes in many clinical applications. In this paper, we first review the fundamental causes of metal artifacts, categorize metal object types, and present recent trends in the CT metal artifact reduction (MAR) literature. To improve image quality and recover information about underlying structures, many methods and correction algorithms have been proposed and tested. We comprehensively review and categorize these methods into six different classes of MAR: metal implant optimization, improvements to the data acquisition process, data correction based on physics models, modifications to the reconstruction algorithm (projection completion and iterative reconstruction), and image-based post-processing. The primary goals of this paper are to identify the strengths and limitations of individual MAR methods and overall classes, and establish a relationship between types of metal objects and the classes that most effectively overcome their artifacts. The main challenges for the field of MAR continue to be cases with large, dense metal implants, as well as cases with multiple metal objects in the field of view. Severe photon starvation is difficult to compensate for with only software corrections. Hence, the future of MAR seems to be headed toward a combined approach of improving the acquisition process with dual-energy CT, higher energy X-rays, or photon-counting detectors, along with advanced reconstruction approaches. Additional outlooks are addressed, including the need for a standardized evaluation system to compare MAR methods.

INDEX TERMS Biomedical imaging, computed tomography, radiation therapy, reconstruction algorithms, metal artifact reduction.

I. INTRODUCTION

Ever since the first computed tomography (CT) scan in the early 1970s [1], the effort to improve image quality for clinical applications has been persistent. A long-standing culprit in the degradation of image quality is the metal object, such as a dental filling, artificial hip, spine implant, or surgical clip. Metal objects in the field of view will strongly attenuate x-rays or even completely block their penetration, resulting in corrupt or missing projection data received by the detector. When an image is reconstructed using this incomplete data, it leads to unnatural changes in appearance, known as artifacts, which are often observed as bright or dark streaks in the image. Errors in CT number throughout the image affect diagnostic ability and hinder accurate distinction of tissue types. This is particularly detrimental in radiation therapy planning for cancer treatment, where inexact tumor localization and characterization of surrounding tissues can propagate to dose calculation errors that severely affect treatment success [2]. Another clinical area in which metal artifacts are a major impediment is orthopedics, due to the high image quality that is required very close to metal implants [3]. To overcome artifacts in CT caused by metal objects, extensive research and development efforts have been devoted to metal artifact reduction (MAR) over the past four decades.

Metal artifacts are common in clinical images and are caused by several mechanisms, most prominently beam hardening, scatter, noise, and the non-linear partial volume (NLPV) effect [4], [5]. Beam hardening occurs in

polychromatic x-ray beams when the average beam energy increases (''hardens'') due to lower-energy photons being more easily absorbed by matter. This phenomenon is more pronounced in the presence of high atomic number materials, including metals, which greatly attenuate low-energy x-rays. As the beam hardens, the physics of transmission change. The remaining photons with higher average energy have subsequent attenuation dominated by Compton scattering, which alters the path of x-rays and causes transmitted photons to hit the detector off the centerline of the incident beam [6]. Both beam hardening and scatter result in more photons reaching areas of the detector where they normally would not be, leading to an underestimation of the attenuation coefficient. Hence, a metal object leads to dark bands or streaks in the image along the axis of greatest attenuation, typically sandwiched by bright overshoots, while the metal object itself will still show up white.

Noise also contributes to metal artifacts in CT. Photon flux measured by CT detectors approximately follows a Poisson distribution, so low photon counts will cause higher relative statistical errors in associated regions of the detector [7]. In addition, detector electronic noise dominates the measurements at very low signal levels. These errors are random, and therefore present as thin dark and bright streaks in the image [4].

The fourth significant cause of metal artifacts is the NLPV effect. This arises when the edge of a metal object straddles certain projection lines, causing a variation in the attenuation coefficient perpendicular to the x-ray propagation direction. Since the intensity of this region measured by the detector is no longer a linear function of attenuation, inconsistencies arise in the projection data, resulting in density estimation errors in the image [8].

An additional artifact cause that stems from data sampling rather than data inconsistency is aliasing. This occurs when the Nyquist-Shannon sampling theorem is not satisfied and the measurement interval between projections is too large. Theoretically, projection data should be sampled at half of the detector cell width or less to avoid aliasing [7]. Undersampling will lead to overlap in the measured frequency spectra, and high-frequency components will not be discernible, leading to streaks near object edges. While some low-level aliasing may always exist, it only presents as visible image artifacts when associated with high-density objects, especially metal objects.

There are many existing MAR techniques that address the above-mentioned artifact causes in various ways. In this review, we perform a thorough review and classification of MAR methods from journal articles, conference proceedings, and patents over the past 40 years. Although not every single approach is included, we have selected nearly all contributions of novel techniques that are well-known in the field, or at least were at their time of introduction, based on the number of citations and the publication journal/conference. Our classification scheme defines six major classes of procedures: (1) The most obvious way of reducing metal artifacts in CT is to prevent them from occurring in the first place, which can be achieved by using non-metal implants or removing metal from patients before scanning. Unfortunately, this is not a realistic option in most cases, so correction further into the imaging process is needed. (2) The next chance for minimizing artifacts is in the data acquisition phase, where modifications can be made to x-ray tube parameters, the detector, and the scan geometry. Multiple energies can also be employed to obtain information at different x-ray spectra. Although these adjustments increase the intrinsic fidelity of the data, MAR with only scan acquisition adjustments still does not yield sufficient image quality in many clinical applications, so (3) the raw data must be corrected and/or the reconstruction algorithm must be improved. These correction- and reconstruction-based MAR approaches are by far the most widely researched. Models of beam hardening, scatter, noise, and other physical causes of artifacts can be applied to correct raw data so that they more accurately represent the ideal line integrals. If the quality of the data is so poor that physics corrections are ineffective, (4) complete replacement of projections can be performed, or an (5) iterative reconstruction can be used that down-weights or ignores the corrupt data. Lastly, if raw projection data is not accessible, (6) MAR can be implemented through post-processing of the reconstructed images, such as filtering or normalization. There are several hybrid procedures that combine techniques and algorithms from multiple categories, but we classify these in the section that best defines the primary innovation of the method.

This review aims to provide a comprehensive presentation and discussion of existing MAR techniques and algorithms, spanning from 1978 to the present. The purpose of this endeavor is to define the current limitations and offer insight into the future directions of the field for overcoming these challenges. An overview of trends in the literature (Figs. 1, 2, 3) gives a general idea of where the field is

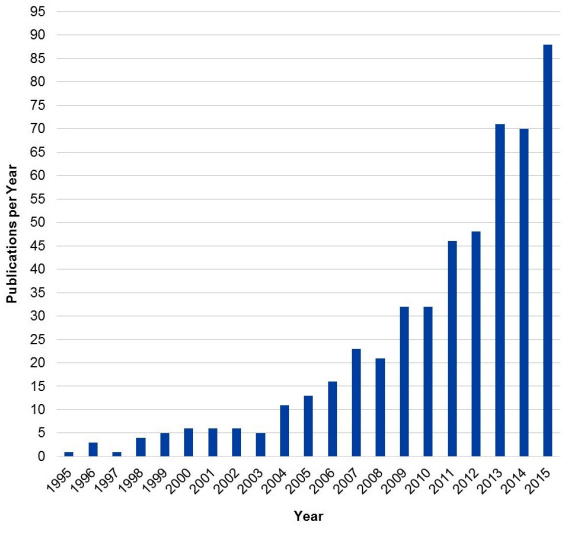

FIGURE 1. Total annual publications on CT MAR during the period of 1995 to 2015. Data obtained from Web of Science™ using keywords "CT metal artifact reduction."

headed. The total number of annual publications related to CT MAR in 2015 has nearly tripled since 2010, as shown in Fig. 1. An increase is certainly expected due to the ''publish or perish'' mentality in academia, but nevertheless the upsurge is substantial. This growth in research indicates the large effort towards adequate MAR solutions for all applications. In particular, since 2010, more MAR papers have been published related to hip and dental implants than spine and cardiac applications, as illustrated in Fig. 2. Very recently, there has been an uptick in the amount of MAR papers related strictly to the topic of radiation therapy, which shows it is gaining momentum as an area in need of better techniques for improved image accuracy. Roughly 20% of the CT MAR publications in 2015 were concerned with radiation therapy applications, which is second only to dental implants (24%).

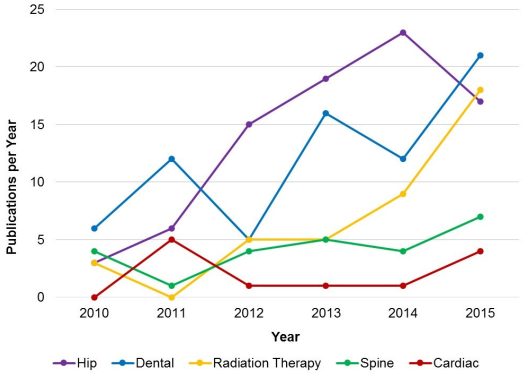

FIGURE 2. Annual publications on CT MAR for hip, dental, radiation therapy, spine, and cardiac applications from 2010 to 2015. Data obtained from Web of Science™ using keywords "CT metal artifact reduction" AND the field, such as "hip." It should be understood that the same paper may be counted among multiple categories if it addresses multiple applications.

A look at the most-cited paper in each of four MAR method categories can reveal information on the technical trends. The most-cited *Projection Completion* publication is ''Reduction of CT artifacts caused by metallic implants'' by Kalender *et al.* (1987), which is a benchmark linear interpolation algorithm to which many new MAR methods are compared. Among *Iterative Reconstruction* algorithms, ''Iterative deblurring for CT metal artifact reduction'' by Wang *et al.* (1996) has the most citations, as a method that explicitly discards data through the metal object and estimates new projections with a deterministically interpreted expectation maximization formula. The most heavily cited *Physics-based Pre-processing* MAR paper is ''Generalized multi-dimensional adaptive filtering for conventional and spiral single-slice, multi-slice, and cone-beam CT'' by Kachelriess *et al.* (2001), which employs adaptive filtering to suppress noise. Finally, the *Acquisition Improvement* category is represented by a paper that managed to reach 100 citations within four years after publication. ''Metal artifact reduction by dual energy computed tomography using monoenergetic extrapolation'' by Bamberg *et al.* (2011) is a dual-energy CT (DECT) protocol that overcomes beam hardening artifacts and generates monoenergetic images.

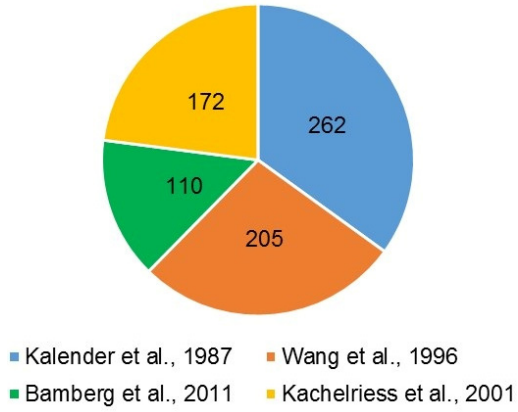

FIGURE 3. The most-cited paper in each of four MAR method categories (with total citation numbers indicated), including *Acquisition Improvement* (Bamberg *et al.*), *Physics-based Pre-processing* (Kachelriess *et al.*), *Projection Completion* (Kalender *et al.*), and *Iterative Reconstruction* (Wang *et al.*). Data obtained from Web of Science™.

All four publications are discussed in further detail in their respective category sections. Fig. 3 reflects the total number of citations for these well-regarded papers. While surveying citation data, it was noted that iterative reconstruction algorithms that account for a physical cause of artifacts have gained more recognition over the past five years, while interpolation algorithms may be falling out of favor for complex applications. Additionally, there has been a rapid rise in popularity of DECT for MAR.

II. METAL OBJECTS

A wide range of metal objects leads to a wide range of CT image artifacts. Depending on the size and material of the implant, different degrees of x-ray attenuation and physics effects will occur. For example, small objects with low density, such as surgical clips, may only cause minor beam hardening or scatter, which can be solved by a physics-based pre-processing correction of the data. Larger and/or denser implants, such as prosthetic hips or dental fillings, will likely require modification of the reconstruction algorithm, either by a projection completion method or statistical iterative reconstruction. Table 1 defines five categories of metal objects, their associated physical and image effects, and the most relevant MAR approaches.

III. METAL ARTIFACT REDUCTION METHODS

The classification scheme in this review defines six major groups of MAR techniques: *Metal Implant Optimization, Acquisition Improvement, Physics-based Pre-processing, Projection Completion, Iterative Reconstruction,* and *Image Post-processing*.

The methods that primarily alter the reconstruction algorithm are discussed under *Projection Completion* and *Iterative Reconstruction*. A standard CT scan acquires projection data of an object at different angles and reconstructs the measurements into an image using filtered back-projection (FBP) or an iterative estimation. The sinogram is

TABLE 1. Categorization of metal implants detailing the types of artifacts and effective techniques for image correction. Adapted from Jin *et al.* [9] with permission.

Category	Definition	Clinical Examples	Physics Effects	Image Effects	MAR Approaches
I	Small metal object, low attenuation	Surgical clip	Minimal beam hardening/scatter	Minor shading in immediate vicinity of metal object	Physics-based correction
II	Medium metal object, medium attenuation	Spinal cage, spinal screw	Beam hardening, scatter, noise, but no complete photon starvation	Moderate bright/dark bands spanning along the directions of highest attenuation	Physics-based correction, Improved acquisition
III	Small metal object, high attenuation	Small dental filling, bullet	Complete photon starvation	Severe bright/dark streaks fanning out from metal object	Projection completion, Iterative reconstruction
IV	Medium/large metal object, portion of the beam with high attenuation	Hip prosthesis	Beam hardening, scatter, noise, and some data with complete photon starvation	Severe bright/dark streaks and thick bright/dark bands over a substantial fraction of the field-of-view	Physics-based correction + projection completion or iterative reconstruction
V	Large metal object, high attenuation	Large and/or multiple dental fillings	Photon starvation	Thick bright/dark bands obliterating a substantial portion of the image	Iterative reconstruction + prior knowledge

the collection of all line attenuation measurements acquired for an image. Since the number of individual measurements is finite, a theoretically ideal image cannot be obtained, but a suitable approximation can be generated using the available data. A metal object in the imaging region causes errors in the projection data mainly due to beam hardening, noise, scatter, or the NLPV effect. Reconstruction using corrupt or incomplete data will result in an image with artifacts. To eliminate these artifacts, many MAR algorithms modify the process by which the image is reconstructed. A common approach is to directly correct or replace the corrupt projection data in the sinogram, such as by interpolation. Another method is to ignore or statistically down-weight data affected by the metal object and employ an iterative procedure to arrive at an image using the more reliable data. Each of these techniques can be improved by pre-processing the data with a model that accounts for a physical cause of the artifacts. Sometimes this correction step is enough by itself and reconstruction modifications are not even necessary. Prior knowledge is an additional consideration that can be applied to projection completion and iterative reconstruction methods. MAR procedures that employ techniques in more than one of the overall categories are discussed within the class that best defines their novelty. The following is an in-depth description of each of these groups and their subclasses, and a detailed presentation of the published methods that comprise them.

A. METAL IMPLANT OPTIMIZATION

The simplest way of reducing metal artifacts in a CT scan is to prevent the presence of metal in the field of view. For clinical applications, this can be crudely achieved by removing metal from the patient or opting for a non-metal implant in the first place. In practice, these options are often not realistic due to the invasive surgery required for implant removal or inadequate metal alternatives. However, a study by Gray *et al.* does show patient cases in which dental fillings were extracted for radiation planning of head and neck cancers [10]. The streak artifacts were completely removed by this extraction, and the ability of physicians to delineate anatomical regions of the head were greatly improved.

Beyond extraction, the majority of studies have focused on assessing image artifacts produced by different types of metal to identify the optimal implant with the least attenuation. Weese *et al.* determined that for surgical clips used

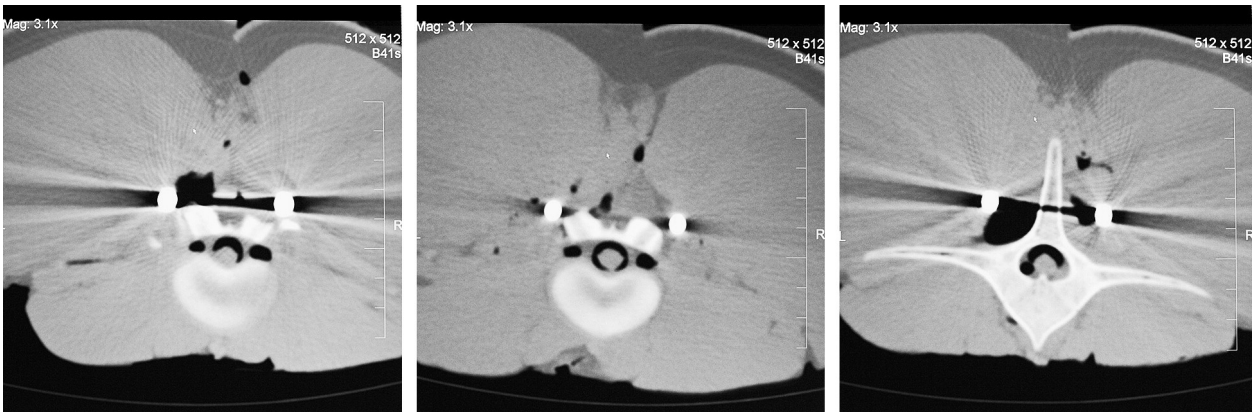

FIGURE 4. Standard clinical CT images of a torso cadaver containing rods of 5.5 mm diameter stainless steel (left), 4.5 mm diameter titanium (middle), and 4.5 mm diameter vitallium (right). Reprinted from Knott *et al.* [15] with permission from Elsevier.

TABLE 2. Mechanical characteristics of patient implant materials relative to each other. Adapted from Knott *et al.* [15] with permission from Elsevier.

Characteristic	Stainless Steel	Titanium	Vitallium
Stiffness	High	Low	Medium
Strength	Medium	High	Medium
Corrosion resistance	Low	High	Medium
Biocompatibility	Low	High	Medium

in hemostasis, those made of titanium and stainless steel produced significantly fewer artifacts than did clips made of tantalum [11]. Further, plastic clips caused no visible artifacts, so they would be ideal from an imaging standpoint, but are limited by ineffective long-term utility. Ebraheim *et al.* later compared stainless steel and titanium in the context of screws and bars for pelvic fixation [12]. Their results revealed that titanium implants substantially reduced image artifacts compared to stainless steel hardware while providing the same level of fixation and quality of fracture healing. A comparison between titanium and cobalt-chrome artificial hips by Haramati *et al.* further confirmed that titanium produced superior image quality, especially in the area directly surrounding the bone [13]. Fig. 4 compares CT image artifacts from rods made of stainless steel, titanium, and vitallium, which is an alloy of cobalt, chromium, and molybdenum that is a candidate to replace titanium. The characteristics of these materials relative to each other are displayed in Table 2. The stiffness of titanium is low compared to stainless steel, which can be a positive or a negative depending on the application. Either way, its higher strength and biocompatibility make titanium an attractive implant option. The titanium rods also produced the lowest degree of artifacts as seen in Fig. 4. Vitallium has a stiffness, strength, and biocompatibility that ranks in between those of stainless steel and titanium, which gives the material more versatility with medium-level characteristics. The image artifacts of vitallium remain a limitation.

In addition to optimizing metal types for reduced artifacts, an exploration into the complementary imaging contrast agents used in DECT was done by Lambert *et al.* [15]. Their work sought contrast enhancement materials that are more compatible for higher energy x-rays. Since one of the x-ray energy spectra used in DECT is typically higher than the x-ray spectrum of standard CT scans, the photons can more easily penetrate metal and lead to fewer inconsistencies in the data. Unfortunately, as beam energy increases, the signal from contrast agents such as iodine or barium diminishes due to their low k-edges. Thus, contrast materials with higher k-edges are more effective with higher average energy beams.

It was shown that tantalum, tungsten, and bismuth preserved contrast signal much better than barium and iodine over the 40 to 140 keV photon energy interval. Barium and iodine signals declined 91-97%, while the higher k-edge group exhibited just a 21-32% reduction in CT number, supporting its potential for use in patients during DECT to complement metal artifact reduction.

Recent exploration has identified magnesium screws as resorbable implants that can interface tissue with bone, and then biodegrade [16]. This material has been shown to maintain its shape and strength while promoting bone growth in mice, with mature bone forming around the implant after three months. Future studies will look at controlling the rate of degradation of the material, which could shape the future direction of patient-level metal artifact reduction. Zimel *et al.* has also explored carbon fiber nails as an alternative to titanium nails for fixating large bones, and found that carbon fiber produced fewer CT image artifacts [17].

Implant optimization within the patient is a basic starting point for MAR, but further reduction measures are necessary to achieve acceptable levels of image quality.

B. ACQUISITION IMPROVEMENT

A second class of strategies is to alter the CT scan acquisition parameters such as x-ray tube voltage, tube current, scan plane, and slice thickness. A more drastic approach is to employ dual-energy protocols that acquire data using two x-ray spectra for material decomposition. Spectral CT with photon-counting is an even different method with the ability to resolve multiple energies from a single spectrum.

1) PARAMETER ADJUSTMENT

Straightforward techniques to improve data acquisition are to simply scan around the metal object or obtain data from preferred gantry angles. A head tilt routine was employed by Brown *et al*. for patients with aneurysm clips so that the axial plane through the clip projected away from the cluster of major cerebral arteries to be evaluated [18]. This method showed that metal artifacts could be minimized in the most important regions of the image by altering the angle of acquisition. A study by Lewis *et al.* later explored gantry tilt angles of 5 to 15 degrees for imaging total knee prostheses [19]. Their results showed that gantry angles of 10 to 15 degrees provided the most accurate mean attenuation values around the implant. Lakits *et al.* then compared helical CT in the axial plane, as well as multiplanar reconstruction of coronal and sagittal images, with conventional CT acquisition in the axial and coronal planes [20]. They determined that a helical acquisition allowed significantly better localization of metal objects and reduced beam hardening artifacts, mainly due to the sagittal plane information, which is not obtainable with conventional CT.

In the context of CT angiography for evaluating vessels around aneurysm clips after placement, Mamourian *et al.* found that axial imaging of titanium and cobalt-chrome implants led to diminished streak artifacts when compared to helical scanning [21]. However, for most applications, the improvement in image quality with axial acquisition is not worth the loss of volumetric coverage provided by helical CT. One unique method presented by Tolakanahalli *et al.* is to obtain digital subtraction angiography-type images using CT with contrast agents [22]. Topographic images are obtained at different angles and the metal objects are subtracted out of the projection data to allow better visualization close to the metal surface.

Other variations to the scan acquisition process have been employed to combat metal artifacts. Link *et al.* extended the CT scale from a maximum window of 4,000 to 40,000 Hounsfield units (HU) to decrease artifacts from femur implants and improve diagnostic power [23]. This extension is beneficial because metal objects with high attenuation coefficients have CT numbers from 8,000 to 20,000 HU, and their values are cut off on standard scanners, resulting in distortion [24]. It was also found that decreasing slice thickness from 5 mm to 2 mm increased diagnostic scores when combined with the extended scale. Moon *et al.* further revealed that smaller slice thicknesses as thin as 0.75 mm led to greatly reduced metal artifacts from stainless steel implants in the femur [25].

A more aggressive approach that has been achieved with ongoing engineering advancements is to increase the voltage (kVp) and/or current (mA) of the x-ray tube so that either higher energy photons or a greater number of photons are generated to penetrate the metal object and surrounding tissue. These modifications inherently increase the quality of the raw data. The Moon *et al.* study also exhibited that higher tube voltage (140 vs 120 kVp) improved artifacts, but higher tube current (500 vs 300 vs. 100 mA) did not have a significant effect on the image quality. Lee *et al.* assessed various protocols for imaging the spine after pedicle screw placement [26]. The tube voltage was varied between 80, 100, and 120 kVp, and the tube current was applied in the range of 60 to 220 mA. As expected, higher voltages led to fewer metal artifacts, but the current variation did not have a significant effect.

The x-ray energy can be increased even more dramatically with a linear accelerator. Schreiner *et al.* acquired images of hip implants using megavoltage CT with photon energies up to 4 mega-electron-volts (MV), which significantly reduced artifacts around the metal surface [27]. The drawback of this technique is increased radiation dose, and so in an effort to reduce the megavoltage exposure, Wu *et al*. integrated select views using MV photon energies into a standard kilovoltage acquisition [28]. The high-voltage data replaces the metal-affected projections in the standard-voltage sinogram so that information lost due to photon starvation is restored. In the context of tomotherapy, Jeon *et al.* employed a similar protocol and showed that images reconstructed from hybrid sinograms containing MV and kV x-ray data had higher contrast-to-noise and signal-to-noise ratios than those from just kV or MV sinograms alone [29]. This, along with decreased metal streak artifacts, allowed for better distinction of relevant structures around implants.

With each adjustment to the scanning procedure that improves metal artifact reduction, there is a disadvantageous side effect. This usually comes in the form of increased radiation dose to the patient or loss of image contrast. Table 3 presents the effects and disadvantages of the acquisition adjustments discussed in this section.

2) DUAL-ENERGY CT

To overcome beam hardening effects, dual-energy CT has been effective because it allows for monoenergetic data sets to be extracted from scans acquired at two separate polychromatic beam spectra. With attenuation coefficients obtained at two energies, monoenergetic images can be synthesized, often referred to as virtual monochromatic spectral (VMS) images. In one of the most highly cited MAR papers over the past five years, Bamberg *et al*. acquired images of metal screws in patients at 100 and 140 kVp, and then extrapolated

TABLE 3. Effects of adjustments to scan acquisition procedure for reducing metal artifacts. Adapted from Lewis *et al.* [30] with permission from Springer.

Acquisition Adjustment	Primary Advantage	Primary Disadvantage
Increase photon energy (kVp)	Reduce beam hardening and noise	Increased patient dose
Increase tube current (mA)	Reduce noise	Increased patient dose
Lower pitch setting	Reduce noise	Increased patient dose
Decrease slice thickness	Reduce partial volume artifact	Increased noise
Extend CT scale	Increased window width & level	Decreased contrast resolution

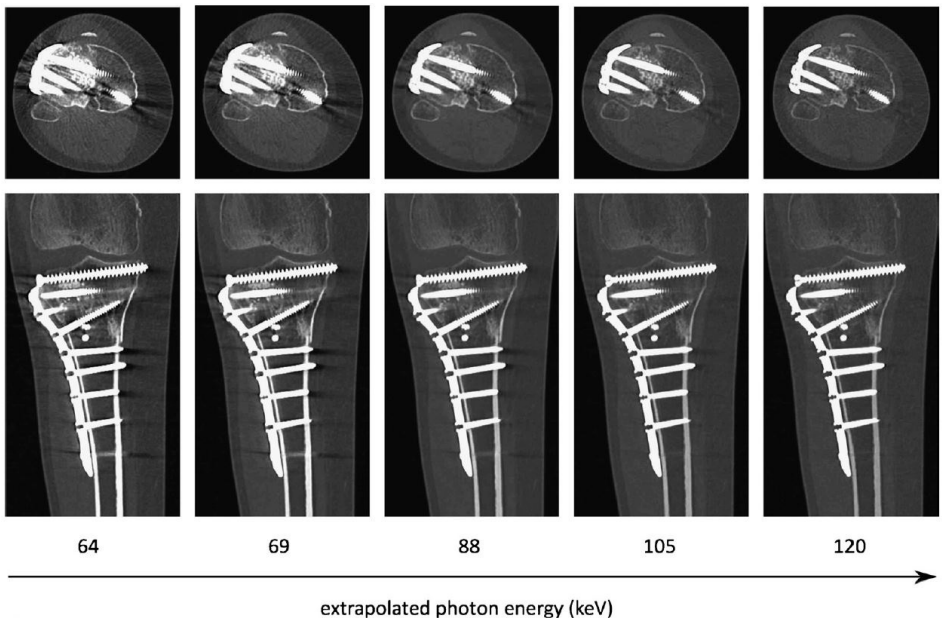

FIGURE 5. Metal artifacts decrease as photon energy increases in single energy extrapolated images from dual-energy CT. Reprinted from Meinel *et al.* [32] with permission from Wolters Kluwer.

the energies of the standard 100 and 140 kVp spectra [31]. This method substantially reduced artifacts by 48.6% at the optimal 119.5 keV energy setting, while increasing diagnostic assessment of the metal surface and surrounding region. They also concluded that 105 keV was an optimal extrapolated energy for visualizing screws.

A later dual-energy CT study by Zhou *et al.* extracted higher photon energies, ranging from 70 to 190 keV, and determined that 130 keV was optimal for reducing metal artifacts [33]. Meinel *et al.* reached similar conclusions when extrapolating single energy images from a dual-energy protocol with 140 and 100 kVp scans [32]. For assessing metal hardware in hip and upper leg bone injuries, the extrapolated energy range of 100 to 130 keV produced the best diagnostic image quality. The median streak intensities decreased from 413 HU at 88 keV to 153 HU at 120 keV, which resulted in improved diagnostic quality of the images. Fig. 5 shows extrapolated VMS images with artifacts decreasing as photon energy increases. However, there are drawbacks at higher energies, including higher radiation dose to the patient. Additionally, Pessis *et al.* showed that image contrast declined beyond a certain energy level, such as 140 keV, and that lower energies around 80 keV were better for detailing soft tissues [34]. A law of diminishing returns in VMS reconstruction was put forth by Lewis *et al.* in the context of hip implant imaging [30]. They extracted 16 single photon energy images between 40 and 190 keV in steps of 10 keV. The results demonstrated that streak artifacts could be reduced with minimal loss of spatial resolution up to 150 keV. Above this threshold, metal artifact reduction is no more effective, and contrast-to-noise ratio decreases. This trend is consistent at tube currents of 100, 200, and 400 mA.

A statistical framework to model noise in dual-energy CT was proposed by Sukovic and Clinthorne [35]. A penalized weighted least squares (PWLS) objective function with constraints in the density domain handles the non-Poisson noise from amorphous silicon (aSi:H) detectors, and is minimized using the Gauss–Seidel algorithm.

This method is compared to the dual-energy FBP counterpart, in terms of bias/standard deviation, and demonstrates advantages in high noise cases, specifically at the low flux rate of 3×10^5 photons/second/detector element (5mm).

3) PHOTON-COUNTING CT

More recently, photon-counting detectors have been considered as a way to reduce metal artifacts. Specifically, photon-counting detectors in charge-summing mode are capable of discriminating individual photon energies for spectral reconstruction and are more efficient at very low photon count levels. Rajendran *et al*. employed a Medipix3RX detector to acquire spectral CT images of titanium and magnesium scaffolds at different energy ranges [36]. Data is reconstructed using the simultaneous algebraic reconstruction technique (SART) that accounts for dead pixels in the detector with oversampling compensation. Images depicting the narrow high energy range of 50 to 80 keV yielded the best metal artifact reduction while preserving contrast.

Nasirudin *et al.* also used a photon-counting detector for spectral CT material decomposition [37]. This information is incorporated into a penalized maximum likelihood reconstruction. Their results showed significant reduction in bright and dark streaks compared to FBP, while structure near metal edges was preserved, as seen in Fig. 6. The proposed method also repeatedly produced attenuation values of teeth and implants that closely matched with theoretical estimates.

C. PHYSICS-BASED PRE-PROCESSING

Physics-based pre-processing techniques aim to model the physical cause of metal artifacts, such as noise, scatter, beam hardening, and the NLPV effect, and correct data in the metal trace to improve reconstruction. These corrections are usually applied in the projection domain before reconstruction, although the same physics models can alternatively be incorporated in the forward model of an iterative reconstruction algorithm.

1) NOISE SUPPRESSION

Hsieh modeled local noise characteristics with an adaptive mean filter [38]. This reduces quantum noise artifacts and streaks while attempting to preserve spatial resolution. Rangayyan and Gordon also combined adaptive filtering with algebraic reconstruction (ART) to suppress streak artifacts [39]. A multidimensional adaptive filtering approach was developed by Kachelriess *et al.* to apply 3D nonlinear filters in the raw data domain [5], [40]. Resolution tradeoffs are smaller as compared to one-dimensional smoothing approaches, as demonstrated with patient data from single- and multi-slice CT to reduce image noise or patient dose. Image noise along most attenuating paths is effectively reduced by 30%–60% in non-cylindrical body regions, such as through the shoulder, with resolution loss below 5%. This method also helps reduce metal artifacts in the hip region.

An improved multi-dimensional adaptive filtering approach was presented by Watzke, where the adaptive filtering strength was adjusted in the shadow of the metal object [41]. Another noise reduction method for hip implant images using directional filtering was implemented by Prell *et al.* [42]. Boas and Fleischmann developed two techniques, metal deletion technique (MDT) and selective ART, which both incorporate an edge-preserving blur filter to reduce noise and streaks [43]. Selective ART also includes a model for noise and beam hardening effects. MDT involves forward projection after the filter, which guides the sinogram completion in metal areas.

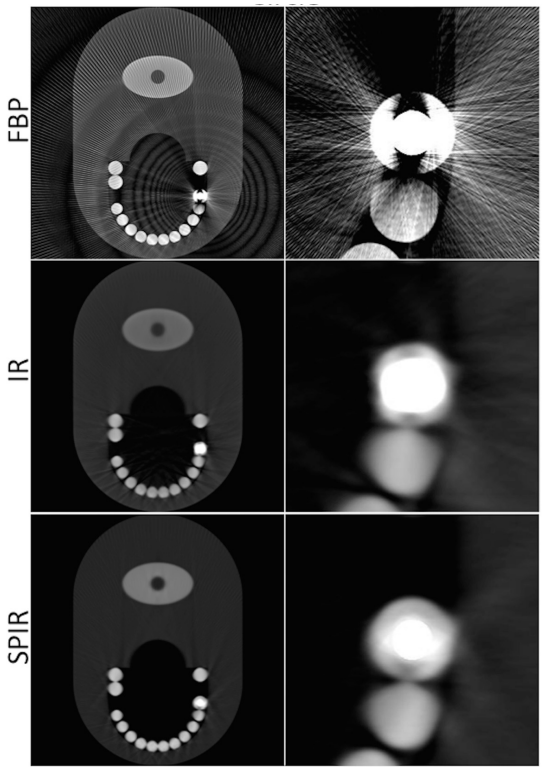

FIGURE 6. Reconstruction results of a dental phantom containing one tooth with a circular metal filling. The novel spectral-driven iterative reconstruction (SPIR) is compared with FBP and the penalized maximum likelihood iterative reconstruction method without prior information (IR). The right column is a zoomed view of the implant in the left column. Reprinted from Nasirudin *et al.* [37].

2) SCATTER AND BEAM HARDENING CORRECTION

Seitz and Rüegsegger improved an interpolation projection completion technique by correcting for beam hardening first and then linearly interpolating corrupt projections [44]. Verburg and Seco presented a novel beam hardening correction for low atomic number implants, such as titanium, that compares projections through the metal with neighboring unaffected projections [45]. For higher atomic number implants, additional iterative reconstruction based on total variation (TV) regularization was applied. Fig. 7 presents the proposed physics correction technique on a titanium spinal implant compared with other common MAR methods. Higher order beam hardening artifacts were approached by Schüller *et al.* without segmentation of the image [46].

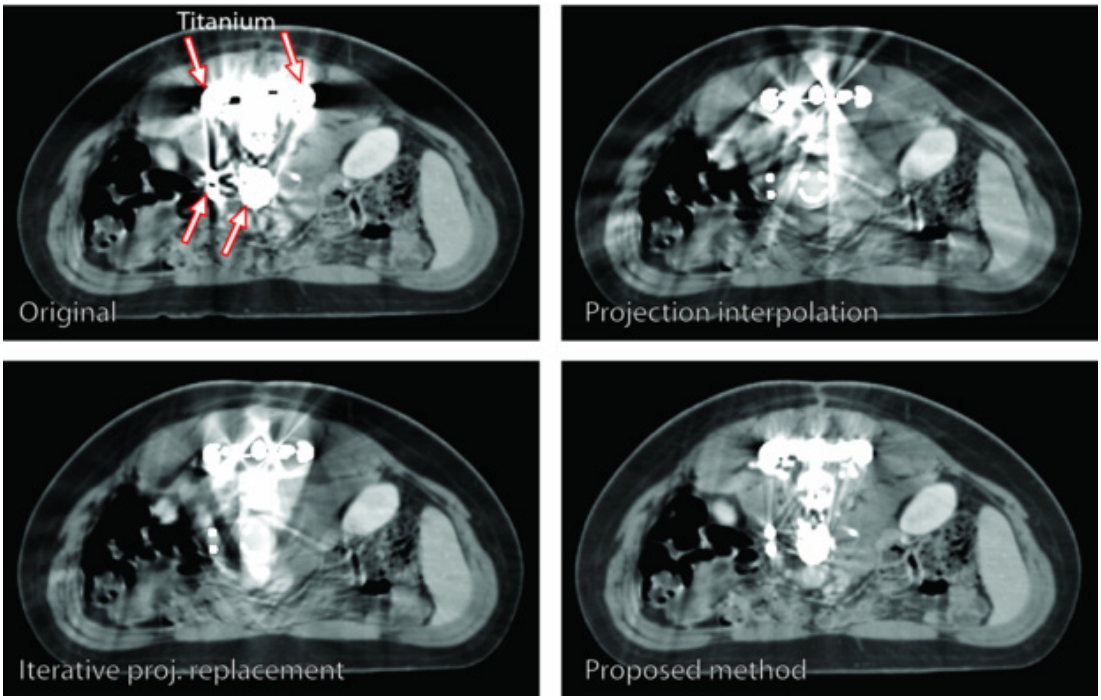

FIGURE 7. Titanium spine implant images show that the proposed beam hardening correction algorithm is more effective than projection replacement techniques alone in reducing streaks and preserving anatomy in the image. Reprinted from Verburg and Seco [45] by permission of IOP Publishing.

To determine where beam hardening correction should be applied, a histogram deformation of the original image is obtained to produce a nonlinear CT value distribution.

For scatter reduction, Meyer *et al.* proposed an empirical scatter correction (ESC) algorithm that makes the assumption that a linear combination of the uncorrected image with various basis images will be scatter-free [47]. The coefficients for the linear combination are calculated by maximizing flatness criteria.

D. PROJECTION COMPLETION

Oftentimes, data in the metal trace are completely corrupt or missing, so new projection data must be synthesized to complete the sinogram. One way to achieve this is by interpolating replacement values, eitehr from neighboring projections or from a mathematical model. We have grouped these as *Interpolation* methods. A second projection completion approach that increases accuracy is to incorporate prior knowledge to guide the estimation of the data that replaces corrupt projections. This prior image is reprojected (forward projected) to generate projection data for sinogram completion, and thus these types of procedures are classified as *Reprojection*.

To improve projection completion processes, some algorithms employ a normalization step that compares raw sinogram data to a prior image sinogram. These techniques are discussed in the *Normalization* section of this class. Projection completion algorithms are the most commonly used and most widely developed form of MAR.

1) INTERPOLATION

The first projection completion method was published by Lewitt and Bates in 1978. Their technique calculates smooth continuations of hollow or truncated projections using either polynomial interpolation or by synthesizing data that satisfies consistency criteria [48]. This criteria is determined by operations on the Fourier coefficients of the projections. The interpolation method is much more straightforward and less computationally intensive, but its success varies on a case-by-case basis, with the highest effectiveness occurring when a small fraction of the projection is hollow, the density distribution is symmetric, or the projection does not change greatly in the interpolated section.

Hinderling *et al.* applied an interpolation technique based on the idea of Lewitt and Bates to reduce metal artifacts when imaging the bone-cement interface of hip implants [49]. They localize the edge of the metal object by finding a sharp discontinuity in the projection gradient, and then create a square wave pseudo-projection between edges of the implant. A linear interpolation of the measured data plus pseudo-projections is used to replace the corrupt projection in the implant interval. Once reconstructed, the image artifacts are suppressed and the distribution of cement and bone can be seen, though the homogeneity is not quite accurate.

Glover and Pelc implemented polynomial completion to address motion streak artifacts from surgical clips [50]. Using a ''rubout'' operation, the projections through the metal object are removed and replaced with data from polynomial

interpolation of neighboring projections. This allows streaks to be eliminated from the image without affecting other areas. One side effect of the method is that nonlinear processing can introduce new artifacts.

Seitz and Rüegsegger developed a consistent completion technique for quantitative CT bone densitometry based on linear interpolation [51]. The computation time for such a protocol is long in complex regions where the solutions to systems of linear equations are not straightforward, although with today's computing power this may no longer be a challenge.

Kalender *et al.* sought a simpler algorithm using linear interpolation [52]. Unlike prior methods that segment metal in the sinogram domain, the boundaries of metal pelvic clips are manually segmented in original corrupt images, and this segmentation is forward projected to identify the corresponding projection data, which are then replaced with interpolated neighboring data. The success of this algorithm depends mainly on the geometric complexity of the metal objects and surrounding anatomy. It was shown to be effective in pelvic regions, but failed when used in the skull due to close areas of high and low attenuation.

Bruyant *et al.* took a different approach to reducing artifacts with interpolation by increasing the number of projections that could be used for image reconstruction [53]. Their algorithm is called interpolation of projections by contouring (IPC), and involves plotting level lines in the sinogram to connect pixels with the same intensity. Interpolation is used to fill in values at all pixels for each level line plot. The data were resampled to multiply the number of projections by 2 or 3, which helped reduce streak artifacts without increasing scan acquisition time.

A more advanced pattern recognition scheme by Morin and Raeside adapted a nearest-neighbor classification to redetermine the transmission values of rays passing through the metal object [54]. Their resulting images were superior to those obtained with simple linear interpolation.

Mahnken *et al.* applied interpolation in a two-dimensional manner by replacing attenuation values of metal-affected sinogram data with the nearest non-corrupt point in the radial direction out of 16 points [55]. If no reliable point is found, the value is weighted to zero. The original segmented metal image is adaptively mixed with the FBP of the corrected projection data to achieve a final image that maintains the object's shape. Moseley *et al.* devised a two-dimensional Taylor series polynomial interpolation MAR method that performed well on small fiducial markers in cone-beam CT [56]. The markers can be completely masked and the values of image voxels in which streaks were present can be reduced to 1% of the original magnitude after correction.

Another polynomial interpolation technique was employed by Wei *et al.* for suppressing metal artifacts near bones [57]. Their ''smoothing-plus-scaling'' procedure isolates bone structures and assigns average CT values to bone pixels in the same region. The metal pixels are replaced with values from polynomial interpolation of neighboring data. All corrected pixels are then added back to the original projection data to reconstruct an image with artifacts suppressed.

Yazdi *et al.* developed an adaptive interpolation algorithm that preserves metal object edges effectively by finding the projection data associated with each edge and maintaining the distance between them [58]. Linear interpolation is performed between these projections to replace the values in the metal implant region. A median filter is applied so that outlier projection values are removed in the implant region. The mean attenuation values and standard deviation in the metal regions of the corrected image were reported to match with that of the original image before metal was inserted.

Veldkamp *et al.* adapted the same interpolation technique in their protocol, but the novelty of their approach was in the metal segmentation by employing a Markov random field to identify affected projections [59]. They also incorporated linear interpolation and Laplacian smoothing for sinogram completion. Yu *et al.* implemented an innovative algorithm that employs a mean-shift technique for highly accurate segmentation of metal objects [60]. Additionally, once the segmentation is forward projected, a feedback-based linear interpolation scheme is used that ensures the calculated values are not larger than the original data they replace. The resulting images of aneurysm clips exhibited a 20-40% reduction in artifacts as measured by standard deviation of surrounding tissue CT numbers.

Projection completion efforts in the wavelet domain have produced more accurate reconstructions in the image regions close to metal objects. Zhao *et al.* presented the first algorithm that performs linear interpolation in segmented metal areas, transforms the sinogram to the wavelet domain, and interpolates between wavelet coefficients to obtain consistent data [61]. This method preserves edges and contrast while keeping the computation time comparable to FBP.

A later technique in the wavelet domain was developed by Mehranian *et al.* that takes advantage of prior wavelet coefficient information of CT sinograms and recovers missing data by solving a regularized inverse problem [62]. It was shown to outperform linear interpolation and the NMAR algorithm based on prior image normalization [63] (discussed in the *Reprojection* section), as illustrated in Fig. 8. Specifically, the proposed technique achieved lower absolute mean deviation values as compared to NMAR in the select regions of interest on the prosthetic hip images. In addition, the technique more effectively removed residual dark streaks.

Liu *et al.* used a sinusoidal curve fitting of the metal-affected projection data instead of line integrals [64], [65]. Only the projections that matched the sinusoidal fit are included for processing, which correspond to the metal object. These projections are amended by subtracting out the attenuation coefficient of the metal to minimize the intensity that will lead to streaks. The new sinogram is reconstructed with reduced artifacts. A more advanced method for accurate structure representation and smooth sinogram filling is to use interpolation based on Euler's elastica as implemented by Gu *et al.* [66]. This technique defines a curvature for

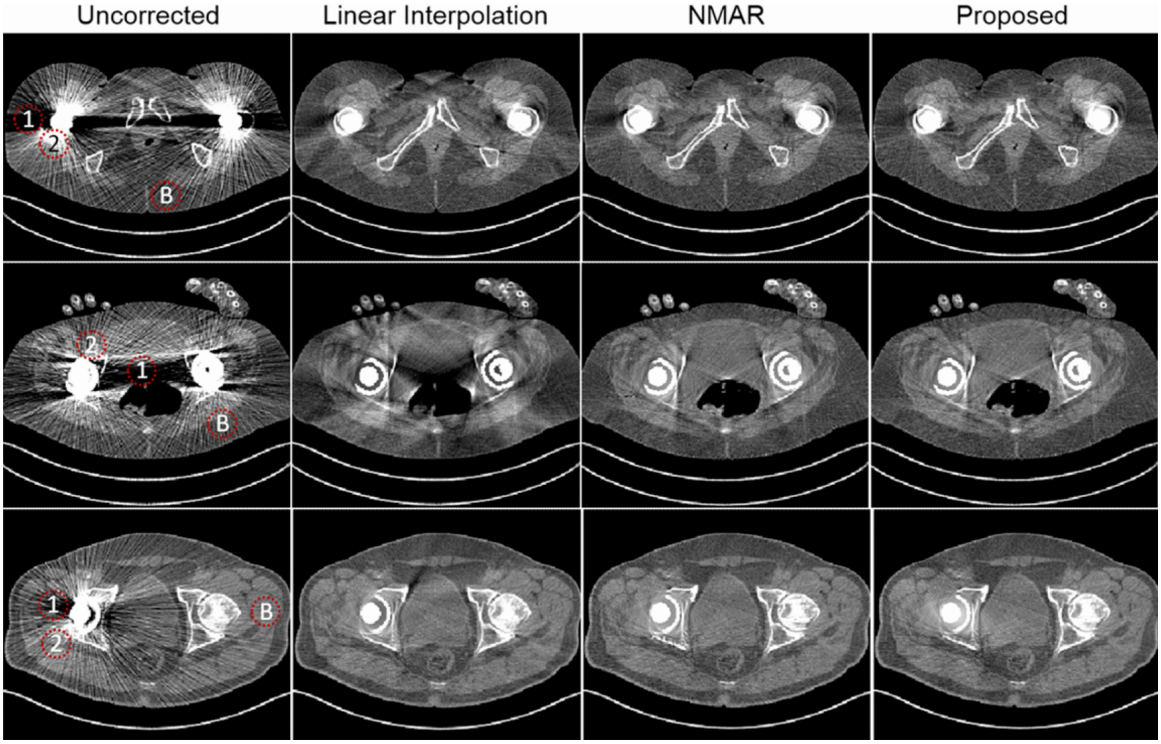

FIGURE 8. Wavelet-domain interpolation optimized by prior information is more effective than interpolation and normalization in reducing residual artifacts. Reprinted from Mehranian *et al.* [62] by permission of IEEE.

inpainting that treats missing data as an occlusion. The resulting images have smoothly connected edges and junctions, though the computation time is greater due to iterative steps.

Zhang *et al*. tried a Laplacian diffusion filter to interpolate metal regions using boundary pixels [67]. The filter is calculated by minimizing the gradient field magnitude surrounding the metal. This method is not effective for large or irregularly shaped objects. Joemai *et al.* also employed 2D Laplacian interpolation for their correction scheme [68]. Kratz and Buzug applied interpolation using non-equispaced Fast Fourier Transforms (NFFT), which allows higher dimension interpolations [69]. Prior knowledge of the metal object can be included in this technique to improve its accuracy.

A novel concept of reformatted projections was tested by Yu *et al.*, which combines projection data at the same view angle over the full longitudinal scan range in helical CT [70]. Two-dimensional interpolation is used to fill the metal segmented projection based on Delaunay triangulation. The method is advantageous for long hip implants because the entire metal region can be captured with reformatted projections. In a similar method, Li *et al*. also employed reformatted projections in helical CT and applied boundary mapping of metal regions along with a dual-front active contour model to track the metal shadow in each projection [71]. This improved their accuracy and led to greater visibility of soft tissue in the corrected images.

Tohnak *et al*. employed a sequential substitution scheme for dental CT to swap corrupt data through fillings with unaffected adjacent projections [72]. Of course, the success of this technique is dependent on a reliable segmentation of the metal objects. To overcome this dependence, Yazdi *et al.* proposed an opposite view replacement method to replace corrupt data with values in the opposite direction of the affected projection [73]. The segmentation is not as crucial for this process because it does not rely on adjacent projections. This is relevant mainly for dental CT or head and neck cancer treatment planning in which there are multiple dental fillings. Xu *et al.* aimed to improve segmentation with the Steger method that detects curvilinear structures for precise determination of small metal object edges [74]. Neighboring projections are used to complete missing data.

A TV inpainting method based on a partial differential equation model was presented by Xue *et al.* [75]. An active contour model is also used for segmenting the metal projection region. Together, the procedure yields a smooth projection completion for dual-energy CT that is reconstructed to produce high quality images for material decomposition. The atomic number of water surrounded by metal objects was measured within 2.3% accuracy with the MAR correction, while measurements without MAR yielded 12.8% error. Zhang *et al.* devised a fractional-order TV inpainting technique that employs a fractional-order gradient parameter for regularization, which handles wide data gaps well [76].

MAR methods for cone-beam CT must deal with 3D reconstruction. Wang *et al.* calculate the 3D coordinates of metal objects and apply a bilinear interpolation to correct

the projection data [77]. Toftegaard *et al.* developed a method for gold radiotherapy markers in cone-beam CT that replaces the markers with linear interpolation, and then reinserts them by 3D trajectory estimation for a final volumetric reconstruction [78].

2) REPROJECTION

Crawford *et al.* developed a reprojection-based method that achieves fast computation time for reducing metal streak artifacts [79]. Their process involves identifying metal objects in an original reconstructed image and filling those regions with the CT number of water. Then, the image is reprojected and those projections are subtracted from the original image projections. The corrected sinogram is reconstructed into the final image. Naidu *et al.* patented a similar process based on this sequence of operations [80]. Tuy developed a method that employs beam hardening correction and then a refinement of projection data by forward projecting the last reconstructed image [81]. The resulting images were enhanced by moderate streak reduction, but new artifacts were introduced around the edges of surgical clips.

Jeong and Ra employed a parallel interpolation protocol that involves reprojecting a metal-free image and merging high-pass and low-pass filtered projection data [82]. The high-pass filtered data is interpolated in regions where multiple metal objects overlap, and this is merged with low-pass filtered data in which the metal projections are replaced with linearly interpolated values. The merged sinogram is reconstructed using FBP, and the resulting images have reduced artifacts with minimal distortion to non-metal regions.

A tissue-class model is a segmentation of different materials that compose the original image, including bone, soft tissue, air, and metal, and is forward projected to be used in the replacement of corrupt projection data. Olive *et al.* developed the first tissue-class model approach for MAR [83]. The initial CT image is segmented into material classes, such as bone, air, metal, and soft tissue, and each region of the same class is assigned a constant value. This image model is forward projected to guide the replacement of corrupt projection data. A difference sinogram is calculated between the class image and original image, and this data is then downscaled and adaptively filtered before final FBP reconstruction. An earlier approach was proposed by Watzke that involved segmenting and separately reprojecting bone regions to avoid introduction of new streak artifacts introduced by the standard interpolation methods [41].

Bal and Spies also implemented an inpainting algorithm aided by an extracted tissue-class model [84]. First, an image is reconstructed and adaptively filtered. Then, the image is segmented using a clustering algorithm. The missing information is estimated via reprojection of the segmented image. In the inpainting stage, either the original sinogram or reprojected sinogram can be completed with data from the tissue-class model. The reprojected sinogram method is particularly advantageous because there is no need for original data. For an optimal completion, the CT number of the metal class is assigned to that of the surrounding material, and residual offsets at the edges are suppressed by correcting the values of the model-derived data segments linearly. This method is compared with the simple linear interpolation method and evaluated with clinical images in which various metal artifacts exist, showing significantly improved image quality and organ contour detectability, which is especially useful for radiation therapy planning.

Lemmens *et al.* devised an interesting algorithm that includes a tissue-class model as well as a model for beam hardening and noise based on maximum a posteriori (MAP) reconstruction [85]. Sole use of multimodal prior image constraints will prohibit streak artifacts, but soft tissue contrast will be compromised at the same time. Hence, in this method the constrained image is only used for projection completion. More specifically, the prior knowledge is available on attenuation coefficients of human tissues. The typical modes are the attenuation coefficients of air, fat tissue, soft tissue, and bone. The intensity priors are defined as Gaussian functions. By using such a prior in combination with a Markov Gibbs smoothing prior, an image can be produced free of streak artifacts. The algorithm was validated with simulations, phantoms, and patient data, and favorably compared with other metal artifact reduction algorithms including the simple linear interpolation method and iterative reconstruction with a polychromatic model.

Prell *et al.* made use of both interpolation and tissue-class model-based reprojection methods to achieve more accurate image reconstructions [86], [87]. An initial three-dimensional interpolation algorithm is used to replace corrupt metal projections, and the sinogram is reconstructed for an intermediate artifact-reduced volume. Next, a tissue-class model is obtained from segmentation that distinguishes air, soft tissue, and bone in this volume, and is then reprojected to directly substitute missing attenuation values in the projection data. A final reconstruction yields a clean, corrected image. A normalization of the raw data relative to the forward projection data is also applied in one of the algorithms to preserve edge information after interpolation [87]. The algorithm achieved an average correction of 1300 HU for CT numbers of metal artifacts, and image noise was reduced by 27%. Fig. 9 displays results of the 3D interpolation algorithm with and without forward projection of the tissue-class model.

Philips Healthcare developed the O-MAR method for orthopedic implants that is based on the reprojections of a metal-segmented image and a tissue-class model derived from the original image with metal removed. All tissue pixels in the tissue-class image are set to a single value [88]. An error sinogram is generated from the difference between the tissue-class sinogram and the original sinogram. This error sinogram is reconstructed to create a correction image.

Karimi *et al.* make use of a prior image derived from segmentation of metal and tissue in the original image [89]. Metal regions are replaced with CT values of soft tissue, and the prior image is reprojected to provide an estimation for the projection data that are used to substitute corrupt projections.

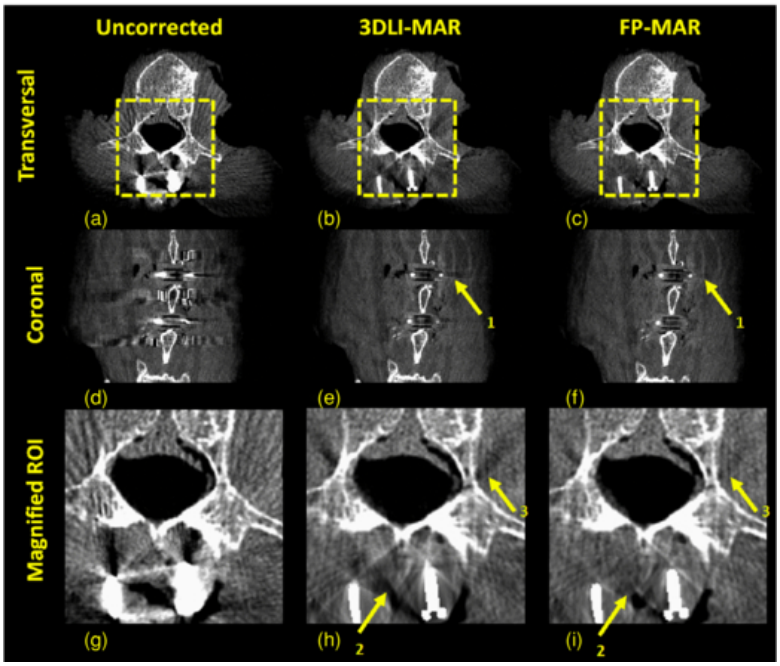

FIGURE 9. Forward projection of a tissue class model combined with 3D interpolation MAR improves image quality better than either method alone. Arrows 1 and 2 illustrate the reduction of the secondary artifacts and better imaging of structures close to the implants. Arrow 3 depicts a clear reduction of interpolation-based artifacts by using the forward projection-based correction. Reprinted from Prell *et al.* [86] by permission of IOP Publishing.

This method was tested on head images containing dental fillings and other small implants, and was effective in preserving anatomical information. For luggage-screening applications of CT, Karimi *et al.* developed a sinogram completion technique that includes constraints for beam hardening, noise, and scatter [90]. A prior-image is created by solving a constrained optimization problem, and the size of this problem is reduced by using smaller artifact-only images. After the optimization of projections, the small images are up-sampled to generate the prior-image, which is then reprojected with metal regions segmented. The sinogram replacement is completed according to the method of Naidu *et al.* [80].

A more accurate prior image for reprojection was sought by Wang *et al.* in their fusion prior-based MAR scheme [91]. This algorithm first corrects the original image projections by linear interpolation of the metal regions, and after reconstruction applies an edge-preserving blur filter to suppress artifacts introduced by interpolation in this pre-corrected image. The CT numbers in the metal areas of the pre-corrected image replace the metal in the original uncorrected image, and the prior image is created by the fusion of these two images. This prior image is forward projected and used to guide the sinogram replacement. The new sinogram values are the result of subtracting the prior sinogram from the original sinogram, performing linear interpolation in the metal trace, and then adding the result to the prior sinogram.

Li *et al.* utilized a prior image generated from the original reconstructed image with an edge-preserving filter applied and replacement of metal with soft tissue CT numbers [92]. The reprojection of this image is used to complete the corrupt sinogram data. Heußer *et al.* proposed a prior-based algorithm that utilizes a planning scan of the same patient before metal implants were inserted or a scan of a similar patient [93]. This image must be coregistered with the measured image that contains artifacts, and then reprojected to be directly used in sinogram completion. This can be a highly effective artifact correction method assuming that an accurate prior image is available.

For cases when an analogous artifact-free scan is not an option, Zhang *et al.* implemented a prior image estimation scheme by imposing TV minimization and a uniformity constraint around the metal objects for algebraic reconstruction of the original projection data [94]. The constrained prior image is then forward projected and combined with smooth interpolations of original projection data to replace corrupt sinogram regions. This hybrid technique shows promising results even for severe metal artifacts. Similarly, Bannas *et al.* employed a prior image obtained using an iterative compressed sensing reconstruction technique [95]. The prior image constrains the estimation of missing information to improve image quality.

3) NORMALIZATION

Data normalization helps to improve the projection completion method for metal artifact reduction. The idea is to use the x-ray path length through a comparable cross-section for

data normalization so that the sinogram becomes comparatively flat and thus more straightforward for interpolation over corrupted metal traces. Müller and Buzug presented one way by first reconstructing an uncorrected image to find metal objects and traces, and then normalizing projections by dividing each measured data point by the intersection length of the corresponding x-ray and the metal object [96]. After interpolation of metal traces, data are denormalized for image reconstruction.

Meyer *et al.* introduced a new type of projection completion technique, called normalized MAR (NMAR), that normalizes original projection data to prior image projection data [63]. An artifact-free prior image is obtained by multithreshold segmentation of the original image after smoothing to define regions of bone, air, and soft tissue. The image is reprojected and the original sinogram is divided by the prior image sinogram. This normalization increases the homogeneity of the regions where linear interpolation will be applied, which leads to more accurate interpolation results. After interpolation, the projection data are denormalized and the corrected data are reconstructed. The normalization and de-normalization procedure fuses original and completed data more smoothly. Image quality measures compared NMAR against the standard linear interpolation and MAR based on simple length normalization for CT scans of hip prostheses, dental fillings, and spine fixation. NMAR can greatly reduce artifacts close to the metal surface even in severe cases, but is dependent on a good prior image with accurate segmentation. This method produces image quality gains and is computationally efficient compared to iterative methods.

The same group improved their method with an adaptive NMAR (ANMAR) algorithm that merges original and NMAR projections using a weighted sum to avoid data loss close to metal objects [97]. Fig. 10 presents the comparison of this method to NMAR and simple linear interpolation (MAR1). Lell *et al.* applied NMAR to clinical cases of head and neck CT to evaluate its performance and found that there were no algorithm-induced artifacts [98].

E. ITERATIVE RECONSTRUCTION

Iterative reconstruction starts with an assumed image and compares its projections to the projection data actually measured by the CT scan acquisition. The goal is then to minimize the error between these sinograms by optimizing an objective function that guides the reconstruction. Examples of this objective function include minimum least squares error and maximum likelihood, which aims to find the distribution of linear attenuation coefficients from the projection data with the maximum probability.

1) CORRUPTION AVOIDANCE

One approach to iterative reconstruction is to completely ignore the subset of projection data that is corrupted by metal objects. These methods treat the MAR problem as the exterior problem, and use data outside the metal trace to arrive at a reconstruction result. The exterior problem gives a unique solution outside the metal object, but is not that stable close to the metal surface.

Medoff *et al.* defined the ''bagel problem'' for MAR, which treats the object being scanned like a bagel with the metal-affected region as the hole in the center [99]. The measurements of x-ray data passing through the hole are completely ignored and only the area outside is reconstructed from unaffected line integrals. The hole is filled in with constant attenuation values, optionally based on the known density of the metal object, and the corresponding line integrals are estimated. An iterative update of the image is performed until steady state is reached. Image quality is improved using this method, though information content at the metal edges is reduced.

Wang *et al.* formulated two iterative deblurring algorithms for metal artifact reduction, using the expectation maximization (EM) formulation and the simultaneous algebraic reconstruction technique (ART) [100]. The objective function is deterministic, meaning it is not directly interpreted in terms of statistics. Corrupted data due to metal are explicitly discarded. The EM procedure defines an initial image estimate and reprojects it to obtain the estimated projections. The measured projection data are divided by the estimated projection data, and then backprojected and multiplied by the current image estimate (pixel by pixel) to generate an improved image estimate. In simulations with noise-free and additive noisy projection data from dental phantoms, both algorithms produced superior image quality as compared to FBP after linearly fitting projection gaps. Furthermore, the EM-type algorithm converges faster than the other algorithm in terms of either the I-divergence or Euclidean distance between ideal and reprojected data. Also, for a given iteration number, the EM-type deblurring method produces better image clarity but stronger noise than the ART-type counterpart. These algorithms were adapted for cone-beam CT with the addition of a 3D relaxation factor that accounts for beam inhomogeneity [101].

The iterative nature of the EM-type algorithm makes it computationally slow relative to MAR methods based on FBP, so Wang *et al.* sought to speed up their method by using row-action/ordered-subsets of the projection data [102]. Each iteration uses only a subset of the data so that the image can be estimated more quickly. The computation time is reduced roughly by a factor equal to the total number of data subsets used. Just four iterations were able to achieve significantly improved image quality.

An inverse iterative procedure was presented by August and Kanade in which a metal mask is generated to isolate projections that need correction [103]. A penalized maximum likelihood method is applied only to the metal mask, which significantly speeds up processing time. The non-metal region is used as a constraint for ensuring corrected data consistency, while smoothness is ensured by a gradient penalty term in the optimization equation. A ten-fold reduction in processing time compared to full image optimization

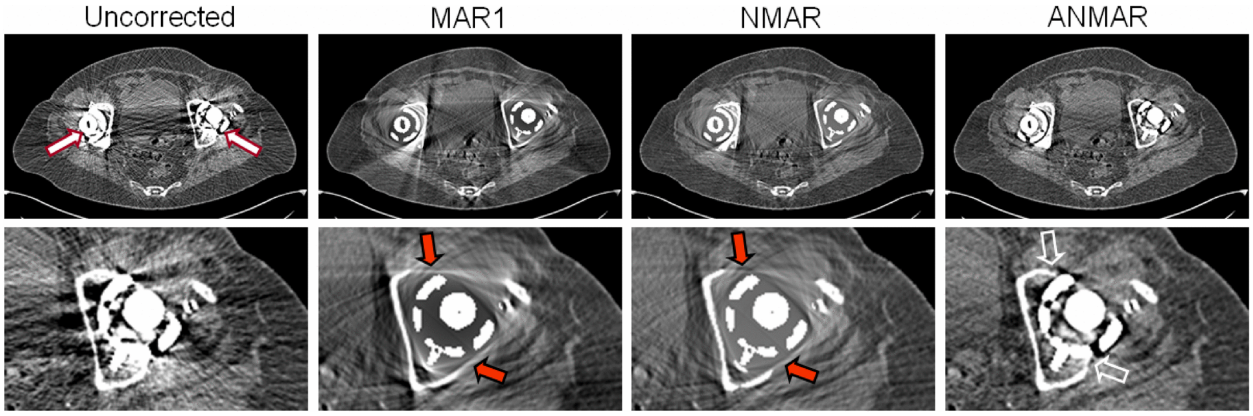

FIGURE 10. Adaptive NMAR achieves more natural images with comparable streak reduction to NMAR. Reprinted from Meyer *et al.* [97] by permission of IEEE.

was seen on images of hip implants, with comparable final results. A similar approach was developed independently by De Man [104].

2) STATISTICAL COMPENSATION

Instead of explicitly omitting metal-affected data, a statistical objective function can be employed that down-weights data through the metal object, but still includes them in the iterative reconstruction.

De Man *et al.* developed a maximum a posteriori algorithm for metal artifact reduction based on the transmission maximum likelihood algorithm (ML-TR) that performs CT reconstruction by optimizing the likelihood of measured Poisson data [105], [106]. Statistically, ML-TR attributes less weight to low-count data, thereby reducing artifacts from directions of low counts due to metal obstacles. This iterative algorithm uses a Markov random field smoothness prior with the Huber potential function. Iterations are performed to produce intermediate images at doubled resolution. The final image is down-sampled to normal resolution. In comparison to the simple linear interpolation method and typical iterative algorithms (ML-TR and ML-EM) ignoring corrupted data, this method produces good results in numerical and phantom tests, reducing streak artifacts and preserving linear details.

A related polychromatic iterative reconstruction approach was proposed by Menvielle, in which a hyperbolic regularization and conjugate gradient optimization is used [107]. De Man *et al.* also incorporated a polychromatic data acquisition model to account for beam hardening into an iterative maximum-likelihood reconstruction algorithm [108]. Like other statistical reconstruction algorithms assuming Poisson data, low-count data are naturally deemphasized. Unlike earlier iterative algorithms, the polychromatic data model reflects the physics most realistically. The polychromatic data-driven iterative reconstruction algorithm prevents beam hardening and metal artifacts, with the spectrum of the x-ray tube modeled as discrete energy bins. The energy-dependent attenuation coefficients are taken into account by decomposing these coefficients into photoelectric and Compton components, under the constraint of relative weight of these components based on prior material assumptions. Good results are obtained in simulations and phantom experiments.

Hamelin *et al.* adapted polychromatic sinogram models that compensate for beam hardening during iterative reconstruction [109]. They also developed a model for Gaussian noise that is appropriate for large average photon counts. These models can be applied on a region of interest basis to account for areas of the image that suffer from different artifacts. A more complex polychromatic beam model was employed by Van Slambrouck and Nuyts, but only in regions of the image close to metal [110]. A patch method is used to determine metal and non-metal regions, and depending on the contents, a simple beam model (MLTRC) or complex model that can also increase resolution (IMPACT) is applied.

The maximum likelihood expectation maximization (MLEM) algorithm assumes a Poisson noise distribution of the projection data and reconstructs the image of linear attenuation values with the highest probability. This particular statistical model is accurate for emission tomography, but not for transmission data in CT. The algorithm weights transmission data incorrectly because the noise on the x-ray path length (post-log) does not follow a Poisson distribution. The MLEM procedure is still advantageous in down-weighting inconsistent projections to suppress metal artifacts, but can be improved for modeling transmission data. Several MAR methods employ this technique for an iterative reconstruction after an interpolation scheme to minimize algorithm-induced artifacts. Oehler and Buzug correct inconsistent projection data by directional interpolation in combination with entropy maximization to obtain appropriate weightings [111]. The directional interpolation method is proposed to fill the data gap following the data flow in the sinogram outside the metal traces, allowing interpolation from data in different projections. This directional method leads to superior results compared to the view-based interpolation schemes. A directional interpolation is recommended with an appropriate weighting to form a weighted maximum likelihood framework for metal artifact reduction, which balances between missing data and residual inconsistencies. A regularization term in the log-likelihood function helps stabilize the model.

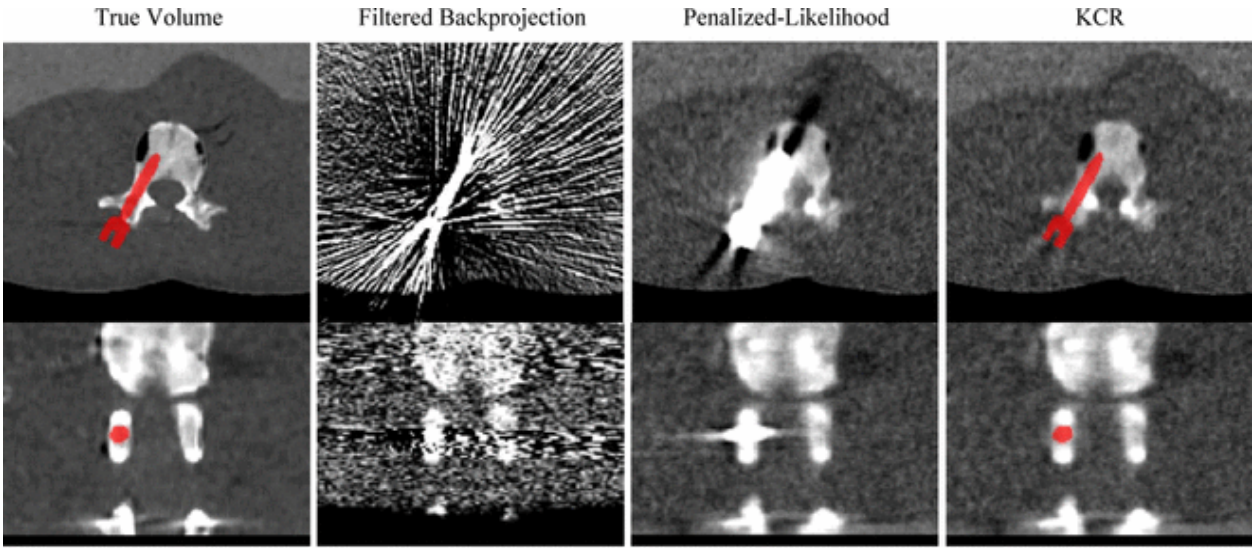

FIGURE 11. KCR estimates the pose of the unilateral single-component screw by simultaneous registration and reconstruction to yield superior image quality to FBP and penalized-likelihood reconstruction. Top: axial view. Bottom: coronal view. Reprinted from Stayman *et al.* [121] by permission of IEEE.

Kratz and Buzug also applied weighted MLEM after NFFT interpolation, which is effective for higher interpolation dimensions [112]. This method can accommodate prior information about the metal object. NFFT helped reduced relative errors based on the ground truth in the image domain by more than 30% compared to linear and cubic interpolation. Aootaphao *et al.* introduced a modified convex algorithm to include a penalty term in the MLEM process, which overcomes noisy images that can result from MLEM alone on ill-conditioned problems [113]. This followed cubic interpolation of metal regions with an offset that allows surrounding bone to be discerned.

Zhang *et al.* use constrained optimization, which minimizes an objective function that preserves smoothness by restricting projection values based on original non-metal projections [114]. The algorithm outperforms ART and EM methods for streak artifact reduction.

3) KNOWLEDGE UTILIZATION

Iterative reconstruction methods involving incomplete data can be improved with further considerations, such as compressed sensing and known component models. With an increased aging population, more and more CT images contain implants, surgical tools, and other metallic objects. A significant opportunity for metal artifact reduction is to use these precisely known physical models. A component model defines the shape, size, and/or density information of the metal objects in the image to help estimate the missing projections. Kalvin and Williamson developed an iterative algorithm that uses a scout image as a prior image for cases when unencoded projection data are not available [115]. The scout image is acquired by keeping the x-ray tube stationary and moving the patient table. Constraints on the corrected image are imposed by scout projection data for consistency and information about the objects in the image, such as size. Kalvin patented a process based on this sequence [116].

Chen *et al.* devised an algorithm to utilize sparsity of an underlying image and generate a realistic prior background through compressed sensing reconstruction from sparse data, which requires only 20 view acquisition angles [117].

An extension of EM-type iterative deblurring by Snyder *et al.* incorporates the shape and attenuation characteristics of the known metal object to improve the iterative reconstruction for intracavitary applicators [118]. O'Sullivan and Benac developed alternating minimization to monotonically decrease the objective function [119]. This technique minimizes the I-divergence between measured and estimated model-based data, which is a reformulation of the maximum-likelihood. Murphy *et al.* aim to estimate the pose of metal implants by using a known component model of the shape and composition [120]. This method employs a steepest descent gradient algorithm to approximate the position and orientation of the objects.

Stayman *et al.* created a model-based penalized-likelihood approach that incorporates a component specification model, and performs an alternating maximization procedure for both the anatomy and the known object inside the patient [121]. This proposed method achieved high quality images in simulated vertebral pedicle screw reconstructions. Fig. 11 compares image quality of known-component reconstruction (KCR) with FBP and penalized-likelihood for an image containing a pedicle screw.

F. IMAGE POST-PROCESSING

A less popular MAR approach is to perform post-processing, which aims to correct in the image domain. Post-processing methods reduce artifacts after the image has been reconstructed, and do not rely on access to raw projection data. These techniques alone are often not as effective

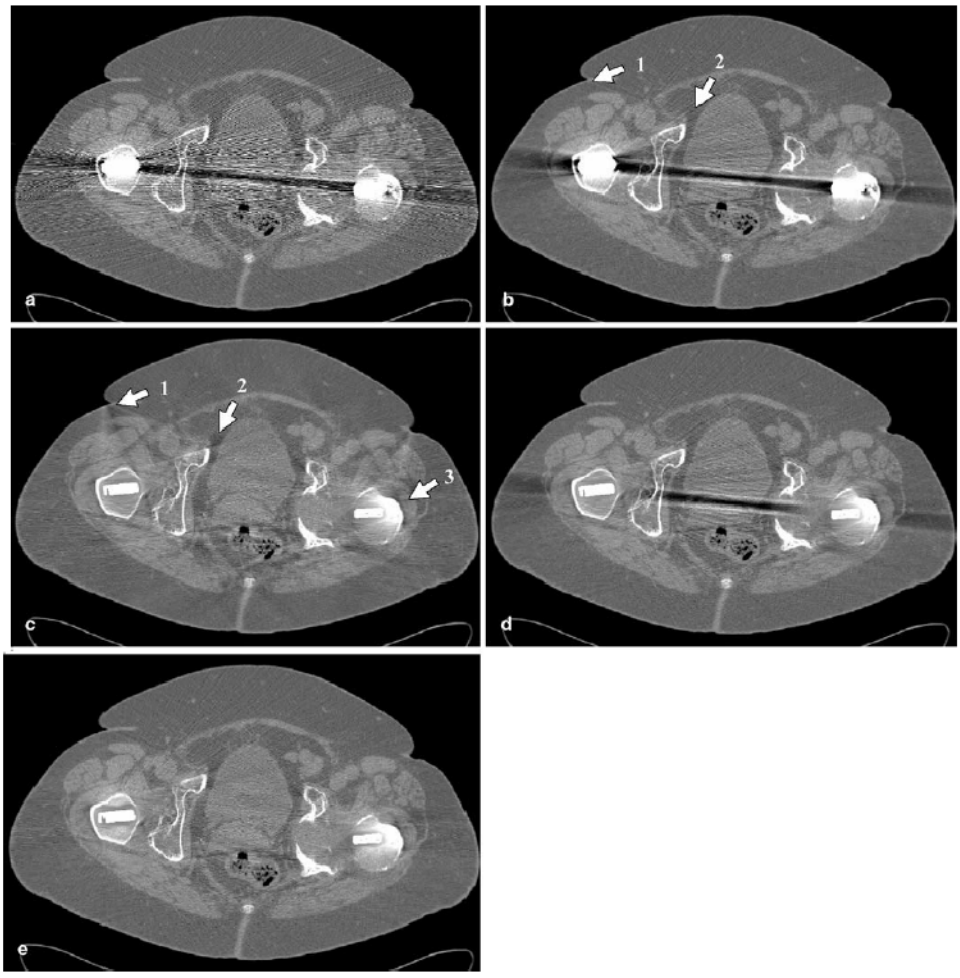

FIGURE 12. Images of two cobalt-chrome hip implants with strong artifacts between them. a) Original; b) MAF; c) Linear interpolation (LI); d) LI-MAF merging with distance weighting; e) LI-MAF merging with directional weighting. Merging with directional weighting significantly improves image quality and minimizes secondary artifacts. Reprinted from Watzke and Kalender [125] with permission from Springer.

as raw data correction approaches since the damage already occurred, but combining post-processing with reconstruction modifications may have merits, as seen with some methods discussed in this section.

1) DIRECT

Direct post-processing for streak reduction was attempted by Henrich with minimal effectiveness [122]. This includes a simple normalization of rows and columns to a gray value. Soltanian-Zadeh *et al.* identified streak artifacts by thresholding a difference image between original and low-pass filtered images and removed them successfully in brain phantom images [123]. For images with mild artifacts, Bal *et al.* employed a radial adaptive filter that acts only on artifact regions of the reconstructed image while preserving spatial resolution elsewhere [124]. The filter is derived from the local structure tensor at each pixel.

2) HYBRID

For more effective results, post-processing has been integrated with other categories of MAR techniques. Watzke and Kalender proposed to combine two artifact reduction methods via image-based weighted superposition of two versions of an image obtained using different MAR methods, the simple linear interpolation method and the multi-dimensional adaptive filtering (MAF) method [125]. The two techniques have their strengths and weaknesses, since they were designed based on different considerations. The linear interpolation method does not use corrupted data, thereby reducing beam hardening and image noise. However, this method often introduces new artifacts. On the other hand, the MAF method greatly suppresses image noise, but it does not effectively reduce artifacts. The synergy among the two methods is clearly shown with patient data that leads to superior image quality than what can be obtained from either method alone. The outcomes achieved with directional weighting are generally preferred over those with the distance weighting. Fig. 12 illustrates the merging of linear interpolation and MAF images, and the image quality improvement with directional weighting.

Meyer *et al.* further introduced a frequency split MAR protocol that combines high frequency information

of the original image to preserve edge data with low frequency information of the image corrected by NMAR [126]. A weighting scheme is used to optimize high frequency data containing edge information without including excess noise in the final reconstructed image.

A baggage screening MAR technique was presented by Mouton *et al.* in which projection completion is combined with post-processing [127]. Metal projection data are replaced by spline interpolation of neighboring projections and the corrected sinogram is reconstructed. The resulting image is then processed to reduce artifacts introduced by interpolation. The pixel values are constrained so that they cannot exceed their value in the original image to avoid bright streaks. More recently, Ballhausen *et al.* combined CT volumes acquired at different tilt angles and computed the average gray values from each volume for regions in space that had artifacts present in some volumes and not others [128]. This helped strongly reduce streaks and improved visual details near metal objects.

IV. DISCUSSION AND CONCLUSION

Oftentimes, different MAR approaches have their unique niches. Table 4 summarizes the detailed assessment of MAR methods described in Section 3 by establishing their relationship to the metal objects whose artifacts they were intended to overcome. Projection completion algorithms make up the majority of MAR techniques, and are primarily targeted to correct artifacts from large and/or highly attenuating metal objects, such as prosthetic hips and dental fillings. There are also several iterative reconstruction algorithms developed for reducing artifacts from these types of implants. For smaller and less attenuating metals, improvements to the acquisition protocol or physics-based pre-processing correction may be sufficient, as there are several methods in these classes geared to those implant categories.

Despite four decades of effort toward reducing metal artifacts in CT (starting with Lewitt and Bates in the late 1970s [48]), there are important applications in which metal objects remain troublesome. In light of Table 4, we underline that larger, irregular metal parts remain challenging, and hybrid iterative reconstruction is the main approach to utilize physical models and minimize metal artifacts.

As a first step for many MAR algorithms, metal segmentation is performed on a first-pass reconstruction image. Due to severe beam-hardening or photon starvation, it is rather difficult to have an accurate segmentation, especially close to the metal surface. Huang *et al.* performed a thorough study of three commercially available MAR techniques on phantoms corresponding to different types of metal implants [129]. These methods are 1) the O-MAR algorithm by Philips Healthcare, which is an iterative projection replacement technique based on a tissue-class model, 2) the monochromatic gemstone spectral imaging (GSI) protocol by GE, which employs dual-energy acquisition at 80 and 140 kVp, *without* any MAR software and 3) the GSI protocol *with* additional MAR software. For the case of large hip implants, GSI with software correction achieved the best artifact reduction results due to the decrease in beam hardening effects facilitated by dual-energy acquisition. More complex phantoms, such as dental fillings, presented a challenge for all three MAR techniques, characterized by the production of additional artifacts in the image without major reduction of the original streaks. For titanium rod spinal implants, all software algorithms induced streaks between the metal objects and the imaging target, which was the lung. These results highlight the limitations of existing MAR methods. Although the O-MAR algorithm is intended for orthopedic implant applications, Kidoh *et al*. tested it strictly for dental fillings and determined that it does have utility in improving image quality, but it cannot effectively overcome streak artifacts [130]. Radiologists assessing images of head and neck tumors in patients with fillings concluded that O-MAR improves the depiction of the oral cavity, but it causes unnatural texture in the images.

To optimize metal artifact reduction, important information could be extracted from data segments compromised by metal objects. It is emphasized that such data segments could be improved using multi-energy scanning techniques, which can effectively facilitate metal artifact reduction. Other prior information in terms of expected image domain knowledge is useful as well. A most immediate objective of MAR is to improve the fidelity of the acquired data so that segmentation quality can be optimized and advanced correction algorithms may not be as necessary. Higher tube voltages generate higher energy x-rays that can penetrate dense metal objects and increase the inherent quality of the raw data. Multiple-energy protocols, high-energy sparse view acquisition, and photon-counting spectral CT have emerged as promising techniques to overcome beam hardening and photon starvation artifacts that result from x-rays passing through metal objects. A high-kVp dual-energy protocol has been proposed by Xi *et al.* in which sparse views at 160 kVp, or even 170 kVp, are acquired intermittently during a standard 120 kVp scan [131]. The data obtained at higher energy suffer from less beam hardening and photon starvation effects, thereby providing adequate projections that can replace corrupt projections through metal objects acquired at the standard energy. Simulation data of this process has shown high image quality close to the metal surface, and is a viable option for improving radiation therapy planning.

Model-based iterative reconstruction is also a promising research direction for reducing metal artifacts [132], [133]. This general class of algorithms incorporates models of physics and materials that help improve the consistency and relevance of x-ray data. System models account for the polychromatic spectrum of the x-ray tube, statistical noise models adjust for the size of the focal spot and detector shape, and prior models constrain the data to only realistic representations of the image. Compressed sensing methods can be considered under prior models in that they use known properties such as sparsity, low-rank, and dictionaries to guide the reconstruction when insufficient data

TABLE 4. Relationship between representative publications in each MAR method class and the categories of metal objects for which they are intended to correct.

	METAL OBJECT CATEGORY				
	I	II	III	IV	V
Acquisition Improvement	Brown[18], Mamourian[21], Lakits[20]	Bamberg[31], Lee[26], Link[23], Meinel[32]	Jeon[29]	Lewis[19], Pessis[34], Schreiner[27]	Nasirudin[37], Wu[28]
Physics Pre-Processing		Verburg[45]	Verburg[45], Meyer[47], Schuller[46]	Prell[42], Kachelriess[40], Meyer[47], Van Slambrouck[110]	
Projection Completion	Glover[50], Kalender[52], Yu[60], Moseley[56], Toftegaard[78], Xu[74], Prell[86], Prell[87], Tuy[81]	Meyer[97], Olive[83], Philips O-MAR[88], Prell[86]	Kratz[69], Jeong[82]	Hinderling[49], Zhao[61], Mahnken[55], Joemai[68], Li[71], Mehranian[62], Veldkamp[59], Yazdi[58], Bal[84], Bannas[95], Meyer[63], Philips O-MAR[88]	Mehranian[62], Tohnak[72], Yazdi[73], Lemmens[85], Meyer[63], Zhang[94]
Iterative Reconstruction		Stayman[121], Snyder[118], Murphy[120]	Wang[100], De Man[105]	August[103], Kalvin[115], Wang[102], Oehler[111]	Oehler[111]
Image Post-Processing	Bal[124]		Watzke[125], Meyer[126], Ballhausen[128]	Watzke[125], Meyer[126]	

is available from the acquisition process. Complementary data from other imaging modalities has also been shown to reduce CT metal artifacts in a unique way. Tri-modality imaging systems that perform CT, MRI, and positron emission tomography (PET) in a single session can acquire synergistic information for image correction as demonstrated by Delso *et al* [134].

A common observation in MAR papers is that the results of a proposed technique are often compared to results obtained using the simple linear interpolation algorithm. Unsurprisingly, nearly every new approach is far superior to this benchmark. To improve synergy in the MAR field and compare many techniques to each other, there is a need for better benchmarks and metrics. Reconstruction algorithms ought to be run on identical data from the same acquisition process. For techniques that alter the scan procedures, identical phantoms should be available. Phantom templates could be shared in a database, downloaded, and 3D printed so that there is common ground for comparison. These phantoms also cannot be too simple, otherwise the complex cases of metal objects are not represented. Testing also needs to include task-based evaluation to assess clinical impact, such as radiation therapy planning. An additional point is that many MAR algorithms require access to raw projection data, but these often cannot be implemented on commercial CT scanners due to restrictions.

In recent years, public concerns over x-ray radiation dose have led to great progress in low-dose CT. Sub-milli-Sievert

scans are becoming common. As a result, metal artifacts could become more evident, which will demand more attention to maintain diagnostic performance. For low-dose CT and spectral imaging, photon-counting detectors are emerging that have an inherent benefit for metal artifact reduction, but have yet to be fully explored. Among many relevant clinical tasks, a primary example that heavily relies on successful metal artifact reduction is proton therapy planning. In this case, any residual metal artifacts can significantly compromise therapeutic outcome margins.

From a methodological perspective, metal artifact reduction and local/interior tomography are closely related. Roughly speaking, in the case of metal artifact reduction, portions of data inside a projection profile are unavailable or seriously compromised due to the presence of metal objects. Meanwhile, local/interior tomography targets reconstruction of an internal region of interest (ROI) from purely truncated projection data segments delimited by the ROI (interior tomography), or from these local data segments plus some additional measured and/or extrapolated data along paths outside the ROI (local tomography). Since interior tomography solves the classical interior problem [135], [136], in a good sense metal artifact reduction methods define what we call exterior tomography. Mathematically, exterior tomography allows a unique solution but regularization is needed for stability.

As a side note, the recent news exposure on AlphaGo demonstrates an impressive success of machine learning, and is inspiring for metal artifact reduction [137]. It can be imagined that the above-described benchmark database can be expanded to serve as a source of big data for training so that a machine learning algorithm can be developed to recognize metal artifacts and infer underlying structures. Such an algorithm can be optimized in a task-specific fashion to become a universal intelligent image analyzer. This could be an exciting direction for big-data-driven intelligent metal artifact reduction.

Forty years of research and development have produced effective methods for reducing metal artifacts. Despite these efforts, some metal objects still pose great challenges for MAR, mainly large or irregular prostheses and dense, highly attenuating implants. There is still no universal solution for cases involving these types of metal that demand high image accuracy, especially for proton therapy. To reach this goal, improved acquisition protocols will need to be combined with reconstruction algorithms that account for the relevant physics effects and prior information. This approach fosters collaboration between multiple groups in different disciplines.

In conclusion, multi-energy data acquisition, advanced algorithms, extensive prior knowledge, standardized benchmark datasets, as well as clinical evaluation and validation would synergistically contribute to the most effective techniques for metal artifact reduction in CT.

REFERENCES

[1] G. N. Hounsfield, "Computerized transverse axial scanning (tomography): Part 1. Description of system," *Brit. Inst. Radiol.*, vol. 46, no. 552, pp. 1016–1022, Jan. 1973.

[2] W. Kilby, J. Sage, and V. Rabett, "Tolerance levels for quality assurance of electron density values generated from CT in radiotherapy treatment planning," *Phys. Med. Biol.*, vol. 47, no. 9, p. 1485, Apr. 2002.

[3] D. D. Robertson, P. J. Weiss, E. K. Fishman, D. Magid, and P. S. Walker, "Evaluation of CT techniques for reducing artifacts in the presence of metallic orthopedic implants," *J. Comput. Assist. Tomogr.*, vol. 12, no. 2, pp. 236–241, Mar. 1988.

[4] B. De Man, J. Nuyts, P. Dupont, G. Marchal, and P. Suetens, "Metal streak artifacts in X-ray computed tomography: A simulation study," *IEEE Trans. Nucl. Sci.*, vol. 46, no. 3, pp. 691–696, Jan. 1999.

[5] M. Kachelriess, "Reduktion von Metallartefakten in der Roentgen-computer-tomographie," Inst. Med. Phys., Univ. Erlangen-Nuremberg, Erlangen, Germany, Tech. Rep., 1998.

[6] F. E. Boas and D. Fleischmann, "CT artifacts: Causes and reduction techniques," *Imag. Med.*, vol. 4, no. 2, pp. 229–240, Apr. 2012.

[7] J. Hsieh, *Computed Tomography, Principles, Design, Artifacts, and Recent Advances*. Bellingham, WA, USA: SPIE, 2009.

[8] G. H. Glover and N. J. Pelc, "Nonlinear partial volume artifacts in X-ray computed tomography," *Med. Phys.*, vol. 7, no. 3, pp. 238–248, 1980.

[9] Y. Jin *et al.*, "Feasibility demonstration of high-voltage clinical CT and impact on X-ray penetration through metal objects," *Med. Phys.*, vol. 43, no. 6, p. 3720, 2016.

[10] W. A. Gray, S. Sekaran, J. A. Tanyi, and J. M. Holland, "Implications of dental artifacts on radiotherapy planning for head and neck cancer," in *Proc. Multidisciplinary Head Neck Symp.*, 2012.

[11] J. L. Weese, M. S. Rosenthal, and H. Gould, "Avoidance of artifacts on computerized tomograms by selection of appropriate surgical clips," *Amer. J. Surgery*, vol. 147, no. 5, pp. 684–687, May 1984.

[12] N. A. Ebraheim, R. Coombs, J. J. Rusin, and W. T. Jackson, "Reduction of postoperative CT artifacts of pelvic fractures by use of titanium implants," *Orthopedics*, vol. 13, no. 12, pp. 1357–1358, Dec. 1990.

[13] N. Haramati *et al.*, "CT scans through metal scanning technique versus hardware composition," *Comput. Med. Imag. Graph.*, vol. 18, no. 6, pp. 429–434, Nov./Dec. 1994.

[14] J. W. Lambert, P. M. Edic, P. Fitzgerald, A. S. Torres, and B. M. Yeh, "Complementary contrast media for metal artifact reduction in dual-energy CT," in *Proc. SPIE 9412, Medical Imag., Phys. Med. Imag.*, Mar. 2015, pp. 1–12, paper 941203.

[15] P. T. Knott *et al.*, "A comparison of magnetic and radiographic imaging artifact after using three types of metal rods: Stainless steel, titanium, and vitallium," *Spine J.*, vol. 10, no. 9, pp. 789–794, Sep. 2010.

[16] S. Galli *et al.*, "Osseointegration of resorbable magnesium screws—A SRμCT study," in *Proc. 6th Symp. Biodegr. Met.*, 2014, p. Invit-14.

[17] M. N. Zimel, S. Hwang, E. R. Riedel, and J. H. Healey, "Carbon fiber intramedullary nails reduce artifact in postoperative advanced imaging," *Skeletal Radiol.*, vol. 44, no. 9, pp. 1317–1325, Sep. 2015.

[18] J. H. Brown, E. S. Lustrin, M. H. Lev, C. S. Ogilvy, and J. M. Taveras, "Reduction of aneurysm clip artifacts on CT angiograms: A technical note," *AJNR. Amer. J. Neuroradiol.*, vol. 20, no. 4, pp. 694–696, 1999.

[19] M. Lewis, A. P. Toms, K. Reid, and W. Bugg, "CT metal artefact reduction of total knee prostheses using angled gantry multiplanar reformation," *Knee*, vol. 17, no. 4, pp. 279–282, Aug. 2010.

[20] A. Lakits, R. Prokesch, C. Scholda, R. Nowotny, A. Kaider, and A. Bankier, "Helical and conventional CT in the imaging of metallic foreign bodies in the orbit," *Acta Ophthalmol. Scand.*, vol. 78, no. 1, pp. 79–83, Feb. 2000.

[21] A. C. Mamourian, K. Erkmen, and D. J. Pluta, "Nonhelical acquisition CT angiogram after aneurysmal clipping: *In vitro* testing shows diminished artifact," *Am. J. Neuroradiol.*, vol. 29, no. 4, pp. 660–662, 2008.

[22] R. P. Tolakanahalli, J. E. Medow, J. Hsieh, G.-H. Chen, and C. A. Mistretta, "Reduction of metal artifacts using subtracted CT projection data," in *Proc. SPIE 5535, Develop. X-Ray Tomogr. IV*, Oct. 2004, pp. 636–643.

[23] T. M. Link *et al.*, "CT of metal implants: Reduction of artifacts using an extended CT scale technique," *J. Comput. Assist. Tomogr.*, vol. 24, no. 1, pp. 165–172, Jan./Feb. 2000.

[24] M.-J. Lee *et al.*, "Overcoming artifacts from metallic orthopedic implants at high-field-strength MR imaging and multi-detector CT 1," *Radiographics*, vol. 27, no. 3, pp. 791–803, 2007.
[25] S. G. Moon *et al.*, "Metal artifact reduction by the alteration of technical factors in multidetector computed tomography: A 3-dimensional quantitative assessment," *J. Comput. Assist. Tomogr.*, vol. 32, no. 4, pp. 630–633, Jul./Aug. 2008.
[26] I. S. Lee *et al.*, "A pragmatic protocol for reduction in the metal artifact and radiation dose in multislice computed tomography of the spine: Cadaveric evaluation after cervical pedicle screw placement," *J. Comput. Assist. Tomogr.*, vol. 31, no. 4, pp. 635–641, Jul./Aug. 2007.
[27] L. J. Schreiner, M. Rogers, G. Salomons, and A. Kerr, "Metal artifact suppression in megavoltage computed tomography," in *Proc. SPIE 5745, Med. Imag., Phys. Med. Imag.*, Aug. 2005, pp. 637–645.
[28] M. Wu, A. Keil, D. Constantin, J. Star-Lack, L. Zhu, and R. Fahrig, "Metal artifact correction for X-ray computed tomography using kV and selective MV imaging," *Med. Phys.*, vol. 41, no. 12, p. 121910, 2014.
[29] H. Jeon *et al.*, "Generation of hybrid sinograms for the recovery of kV-CT images with metal artifacts for helical tomotherapy," *Med. Phys.*, vol. 42, no. 8, pp. 4654–4667, 2015.
[30] M. Lewis, K. Reid, and A. P. Toms, "Reducing the effects of metal artefact using high keV monoenergetic reconstruction of dual energy CT (DECT) in hip replacements," *Skeletal Radiol.*, vol. 42, no. 2, pp. 275–282, Feb. 2013.
[31] F. Bamberg, A. Dierks, K. Nikolaou, M. F. Reiser, C. R. Becker, and T. R. C. Johnson, "Metal artifact reduction by dual energy computed tomography using monoenergetic extrapolation," *Eur. Radiol.*, vol. 21, no. 7, pp. 1424–1429, Jul. 2011.
[32] F. G. Meinel, B. Bischoff, Q. Zhang, F. Bamberg, M. F. Reiser, and T. R. C. Johnson, "Metal artifact reduction by dual-energy computed tomography using energetic extrapolation: A systematically optimized protocol," *Invest. Radiol.*, vol. 47, no. 7, pp. 406–414, Jul. 2012.
[33] C. Zhou *et al.*, "Monoenergetic imaging of dual-energy CT reduces artifacts from implanted metal orthopedic devices in patients with factures," *Acad. Radiol.*, vol. 18, no. 10, pp. 1252–1257, Oct. 2011.
[34] E. Pessis *et al.*, "Virtual monochromatic spectral imaging with fast kilovoltage switching: Reduction of metal artifacts at CT," *Radiographics*, vol. 33, no. 2, pp. 573–583, 2013.
[35] P. Sukovic and N. H. Clinthorne, "Penalized weighted least-squares image reconstruction for dual energy X-ray transmission tomography," *IEEE Trans. Med. Imag.*, vol. 19, no. 11, pp. 1075–1081, Nov. 2000.
[36] K. Rajendran *et al.*, "Reducing beam hardening effects and metal artefacts in spectral CT using Medipix3RX," *J. Instrum.*, vol. 9, no. 3, p. P03015, 2014.
[37] R. A. Nasirudin *et al.*, "Reduction of metal artifact in single photon-counting computed tomography by spectral-driven iterative reconstruction technique," *PLoS One*, vol. 10, no. 5, p. e0124831, 2015.
[38] J. Hsieh, "Adaptive streak artifact reduction in computed tomography resulting from excessive X-ray photon noise," *Med. Phys.*, vol. 25, no. 11, pp. 2139–2147, 1998.
[39] R. M. Rangayyan and R. Gordon, "Streak preventive image reconstruction with ART and adaptive filtering," *IEEE Trans. Med. Imag.*, vol. 1, no. 3, pp. 173–178, Nov. 1983.
[40] M. Kachelrieß, O. Watzke, and W. A. Kalender, "Generalized multi-dimensional adaptive filtering for conventional and spiral single-slice, multi-slice, and cone-beam CT," *Med. Phys.*, vol. 28, no. 4, pp. 475–490, 2001.
[41] O. Watzke, "Metallartefakreduktion in der Computertomographie," Univ. Erlangen-Nuremberg, Erlangen, Germany, Tech. Rep., 2002.
[42] D. Prell, Y. Kyriakou, M. Kachelrie, and W. A. Kalender, "Reducing metal artifacts in computed tomography caused by hip endoprostheses using a physics-based approach," *Invest. Radiol.*, vol. 45, no. 11, pp. 747–754, 2010.
[43] F. E. Boas and D. Fleischmann, "Evaluation of two iterative techniques for reducing metal artifacts in computed tomography," *Radiol.*, vol. 259, no. 3, pp. 894–902, 2011.
[44] P. Seitz and P. Rüegsegger, "Anchorage of femoral implants visualized by modified computed tomography," *Arch. Orthopaedic Traumatic surgery*, vol. 100, no. 4, pp. 261–266, Dec. 1982.
[45] J. M. Verburg and J. Seco, "CT metal artifact reduction method correcting for beam hardening and missing projections," *Phys. Med. Biol.*, vol. 57, no. 9, p. 2803, 2012.
[46] S. Schüller *et al.*, "Segmentation-free empirical beam hardening correction for CT," *Med. Phys.*, vol. 42, no. 2, p. 794, 2015.
[47] E. Meyer, C. Maaß, M. Baer, R. Raupach, B. Schmidt, and M. Kachelrieß, "Empirical scatter correction (ESC): A new CT scatter correction method and its application to metal artifact reduction," in *Proc. IEEE Nuclear Sci. Symp. Med. Imag. Conf.*, Oct./Nov. 2010, pp. 2036–2041.
[48] R. M. Lewitt and R. H. T. Bates, "Image-reconstruction from projections. III. Projection completion methods (theory)," *Optik*, vol. 50, pp. 189–204, 1978.
[49] T. Hinderling, P. Rüegsegger, M. Anliker, and C. Dietschi, "computed tomography reconstruction from hollow projections: An application to in vivo evaluation of artificial hip joints," *J. Comput. Assist. Tomogr.*, vol. 3, no. 1, pp. 52–57, Feb. 1979.
[50] G. H. Glover and N. J. Pelc, "An algorithm for the reduction of metal clip artifacts in CT reconstructions," *Med. Phys.*, vol. 8, no. 6, pp. 799–807, 1981.
[51] P. Seitz and P. Rüegsegger, "CT bone densitometry of the anchorage of artificial knee joints," *J. Comput. Assist. Tomogr.*, vol. 9, no. 3, p. 621, 1985.
[52] W. A. Kalender, R. Hebel, and J. Ebersberger, "Reduction of CT artifacts caused by metallic implants," *Radiolgy*, vol. 164, no. 2, pp. 576–577, 1987.
[53] P. P. Bruyant, J. Sau, and J. J. Mallet, "Streak artifact reduction in filtered backprojection using a level line–based interpolation method," *J. Nucl. Med.*, vol. 41, no. 11, pp. 1913–1919, Nov. 2000.
[54] R. L. Morin and D. E. Raeside, "A pattern recognition method for the removal of streaking artifact in computed tomography," *Radiol.*, vol. 141, no. 1, pp. 229–233, Oct. 1981.
[55] A. H. Mahnken *et al.*, "A new algorithm for metal artifact reduction in computed tomography: *In vitro* and in vivo evaluation after total hip replacement," *Invest. Radiol.*, vol. 38, no. 12, pp. 769–775, Dec. 2003.
[56] D. J. Moseley, J. H. Siewerdsen, and D. A. Jaffray, "High-contrast object localization and removal in cone-beam CT," in *Proc. SPIE 5745, Med. Imag., Phys. Med. Imag.*, Apr. 2005, pp. 40–50.
[57] J. Wei, L. Chen, G. A. Sandison, Y. Liang, and L. X. Xu, "X-ray CT high-density artefact suppression in the presence of bones," *Phys. Med. Biol.*, vol. 49, p. 5407, Nov. 2004.
[58] M. Yazdi, L. Gingras, and L. Beaulieu, "An adaptive approach to metal artifact reduction in helical computed tomography for radiation therapy treatment planning: Experimental and clinical studies," *Int. J. Radiat. Oncol. Biol. Phys.*, vol. 62, no. 4, pp. 1224–1231, Jul. 2005.
[59] W. J. H. Veldkamp, R. M. S. Joemai, A. J. van der Molen, and J. Geleijns, "Development and validation of segmentation and interpolation techniques in sinograms for metal artifact suppression in CT," *Med. Phys.*, vol. 37, no. 2, pp. 620–628, Feb. 2010.
[60] H. Yu *et al.*, "A segmentation-based method for metal artifact reduction," *Acad. Radiol.*, vol. 14, no. 4, pp. 495–504, Apr. 2007.
[61] S. Zhao, D. D. Robertson, G. Wang, B. Whiting, and K. T. Bae, "X-ray CT metal artifact reduction using wavelets: An application for imaging total hip prostheses," *IEEE Trans. Med. Imag.*, vol. 19, no. 12, pp. 1238–1247, Dec. 2000.
[62] A. Mehranian, M. R. Ay, A. Rahmim, and H. Zaidi, "X-ray CT metal artifact reduction using wavelet domain L_0 sparse regularization," *IEEE Trans. Med. Imag.*, vol. 32, no. 9, pp. 1707–1722, Sep. 2013.
[63] E. Meyer, R. Raupach, M. Lell, B. Schmidt, and M. Kachelrieß, "Normalized metal artifact reduction (NMAR) in computed tomography," *Med. Phys.*, vol. 37, no. 10, pp. 5482–5493, 2010.
[64] J. J. Liu, S. R. Watt-Smith, and S. M. Smith, "A description for computed tomography based on sinusoidal curves," *J. Xray. Sci. Technol.*, vol. 11, pp. 205–218, Jun. 2003.
[65] J. J. Liu, S. R. Watt-Smith, and S. M. Smith, "Metal artifact reduction for CT based on sinusoidal description," *J. Xray. Sci. Technol.*, vol. 13, no. 2, pp. 85–96, 2005.
[66] J. Gu, L. Zhang, G. Yu, Y. Xing, and Z. Chen, "X-ray CT metal artifacts reduction through curvature based sinogram inpainting," *J. Xray. Sci. Technol.*, vol. 14, no. 2, pp. 73–82, 2006.
[67] Y. Zhang, L. Zhang, X. R. Zhu, A. K. Lee, M. Chambers, and L. Dong, "Reducing metal artifacts in cone-beam CT images by preprocessing projection data," *Int. J. Radiat. Oncol. Biol. Phys.*, vol. 67, no. 3, pp. 924–932, Mar. 2007.

[68] R. M. S. Joemai, P. W. de Bruin, W. J. H. Veldkamp, and J. Geleijns, "Metal artifact reduction for CT: Development, implementation, and clinical comparison of a generic and a scanner-specific technique," *Med. Phys.*, vol. 39, no. 2, p. 1125, 2012.

[69] B. Kratz, I. Weyers, and T. M. Buzug, "A fully 3D approach for metal artifact reduction in computed tomography," *Med. Phys.*, vol. 39, no. 11, p. 7042, 2012.

[70] L. Yu *et al.*, "Metal artifact reduction from reformatted projections for hip prostheses in multislice helical computed tomography," *Invest. Radiol.*, vol. 44, no. 11, pp. 691–696, 2009.

[71] H. Li, L. Yu, X. Liu, J. G. Fletcher, and C. H. McCollough, "Metal artifact suppression from reformatted projections in multislice helical CT using dual-front active contours," *Med. Phys.*, vol. 37, no. 10, p. 5155, 2010.

[72] S. Tohnak, A. J. H. Mehnert, M. Mahoney, and S. Crozier, "Dental CT metal artefact reduction based on sequential substitution," *Dentomaxillofacial Radiol.*, vol. 40, no. 3, pp. 184–190, 2011.

[73] M. Yazdi, M. A. Lari, G. Bernier, and L. Beaulieu, "An opposite view data replacement approach for reducing artifacts due to metallic dental objects," *Med. Phys.*, vol. 38, no. 4, pp. 2275–2281, 2011.

[74] C. Xu, F. Verhaegen, D. Laurendeau, S. A. Enger, and L. Beaulieu, "An algorithm for efficient metal artifact reductions in permanent seed," *Med. Phys.*, vol. 38, no. 1, pp. 47–56, 2011.

[75] H. Xue, L. Zhang, Y. Xiao, Z. Chen, and Y. Xing, "Metal artifact reduction in dual energy CT by sinogram segmentation based on active contour model and TV inpainting," in *Proc. IEEE Nucl. Sci. Symp. Conf.*, Oct./Nov. 2009, pp. 904–908.

[76] Y. Zhang, Y. F. Pu, J. R. Hu, Y. Liu, and J. L. Zhou, "A new CT metal artifacts reduction algorithm based on fractional-order sinogram inpainting," *J. Xray. Sci. Technol.*, vol. 19, no. 3, pp. 373–384, 2011.

[77] Q. Wang, L. Li, L. Zhang, Z. Chen, and K. Kang, "A novel metal artifact reducing method for cone-beam CT based on three approximately orthogonal projections," *Phys. Med. Biol.*, vol. 58, no. 1, pp. 1–17, 2013.

[78] J. Toftegaard *et al.*, "Moving metal artifact reduction in cone-beam CT scans with implanted cylindrical gold markers," *Med. Phys.*, vol. 41, no. 12, p. 121710, 2014.

[79] C. R. Crawford, J. G. Colsher, N. J. Pelc, and A. H. R. Lonn, "High speed reprojection and its applications," in *Proc. SPIE 0914, Med. Imag. II*, pp. 311–318, Jun. 1988.

[80] R. Naidu, I. Bechwati, S. Karimi, S. Simanovsky, and C. Crawford, "Method of and system for reducing metal artifacts in images generated by X-ray scanning devices," U.S. Patent 6 721 387 B1, Apr. 13, 2004.

[81] H. K. Tuy, "A post-processing algorithm to reduce metallic clip artifacts in CT images," *Eur. Radiol.*, vol. 3, no. 2, pp. 129–134, Apr. 1993.

[82] K. Y. Jeong and J. B. Ra, "Metal artifact reduction based on sinogram correction in CT," in *Proc. IEEE Nucl. Sci. Symp. Conf.*, Oct./Nov. . 2009, pp. 3480–3483.

[83] C. S. Olive, M. R. Kaus, V. Pekar, K. Eck, and L. Spies, "Segmentation-aided adaptive filtering for metal artifact reduction in radio-therapeutic CT images," in *Proc. SPIE 5370, Med, Imag., Image Process.*, pp. 1991–2002, 2004.

[84] M. Bal and L. Spies, "Metal artifact reduction in CT using tissue-class modeling and adaptive prefiltering," *Med. Phys.*, vol. 33, no. 8, p. 2852, 2006.

[85] C. Lemmens, D. Faul, and J. Nuyts, "Suppression of metal artifacts in CT using a reconstruction procedure that combines MAP and projection completion," *IEEE Trans. Med. Imag.*, vol. 28, no. 2, pp. 250–260, Feb. 2009.

[86] D. Prell, Y. Kyriakou, M. Beister, and W. A. Kalender, "A novel forward projection-based metal artifact reduction method for flat-detector computed tomography," *Phys. Med. Biol.*, vol. 54, no. 21, pp. 6575–6591, Oct. 2009.

[87] D. Prell, Y. Kyriakou, T. Struffert, A. Dörfler, and W. A. Kalender, "Metal artifact reduction for clipping and coiling in interventional C-arm CT," *AJNR. Am. J. Neuroradiol.*, vol. 31, no. 4, pp. 634–639, 2010.

[88] Philips CT Clinical Science, *Metal Artifact Reduction for Orthopedic Implants (O-MAR) [White Paper]*. Andover, MA, USA: Philips Healthcare USA, 2012.

[89] S. Karimi, P. Cosman, C. Wald, and H. Martz, "Segmentation of artifacts and anatomy in CT metal artifact reduction," *Med. Phys.*, vol. 39, no. 10, p. 5857, 2012.

[90] S. Karimi, H. Martz, and P. Cosman, "Metal artifact reduction for CT-based luggage screening," *J. Xray. Sci. Technol.*, vol. 23, no. 4, pp. 435–451, 2015.

[91] J. Wang, S. Wang, Y. Chen, J. Wu, J.-L. Coatrieux, and L. Luo, "Metal artifact reduction in CT using fusion based prior image," *Med. Phys.*, vol. 40, no. 8, p. 81903, 2013.

[92] M. Li, J. Zheng, T. Zhang, Y. Guan, P. Xu, and M. Sun, "A prior-based metal artifact reduction algorithm for X-ray CT," *J. Xray. Sci. Technol.*, vol. 23, no. 2, pp. 229–241, 2015.

[93] T. Heußer, M. Brehm, L. Ritschl, S. Sawall, and M. Kachelrieß, "Prior-based artifact correction (PBAC) in computed tomography," *Med. Phys.*, vol. 41, no. 2, p. 021906, 2014.

[94] Y. Zhang, H. Yan, X. Jia, J. Yang, S. B. Jiang, and X. Mou, "A hybrid metal artifact reduction algorithm for X-ray CT," *Med. Phys.*, vol. 40, no. 4, p. 041910, 2013.

[95] P. Bannas *et al.*, "Prior image constrained compressed sensing metal artifact reduction (piccs-mar): 2d and 3d image quality improvement with hip prostheses at ct colonography," *Eur. Radiol.*, vol. 26, no. 7, pp. 2039–2046, Jul. 2016.

[96] J. Müller and T. M. Buzug, "Spurious structures created by interpolation-based CT metal artifact reduction," in *Proc. SPIE 7258, Med. Imag., Phys. Med. Imag.*, Mar. 2009, pp. 72581Y-1–72581Y-8.

[97] E. Meyer, R. Raupach, B. Schmidt, A. H. Mahnken, and M. Kachelriess, "Adaptive normalized metal artifact reduction (ANMAR) in computed tomography," in *Proc. IEEE Nucl. Sci. Symp. Conf. Rec.*, Oct. 2011, pp. 2560–2565.

[98] M. M. Lell *et al.*, "Normalized metal artifact reduction in head and neck computed tomography," *Invest. Radiol.*, vol. 47, no. 7, pp. 415–421, 2012.

[99] B. P. Medoff, W. R. Brody, M. Nassi, and A. Macovski, "Iterative convolution backprojection algorithms for image reconstruction from limited data," *J. Opt. Soc. Amer.*, vol. 73, no. 11, p. 1493, 1983.

[100] G. Wang, D. L. Snyder, and J. O'Sullivan, and M. W. Vannier, "Iterative deblurring for CT metal artifact reduction," *IEEE Trans. Med. Imag.*, vol. 15, no. 5, pp. 657–664, May 1996.

[101] G. Wang, M. W. Vannier, and P.-C. Cheng, "Iterative X-ray cone-beam tomography for metal artifact reduction and local region reconstruction," *Microsc. Microanal.*, vol. 5, no. 1, pp. 58–65, 1999.

[102] G. Wang, T. Frei, and M. Vannier, "Fast iterative algorithm for metal artifact reduction in X-ray CT," *Acad. Radiol.*, vol. 7, no. 8, pp. 607–614, 2000.

[103] J. August and T. Kanade, "Fast streaking artifact reduction in CT using constrained optimization in metal masks," in *Proc. Med. Image Comput.-Assisted Intervent. (MICCAI)*, 2004, pp. 1044–1045.

[104] B. De Man, "Method and apparatus for the reduction of artifacts in computed tomography images," U.S. Patent 7 444 010 B2, Oct. 28, 2008.

[105] B. De Man, J. Nuyts, P. Dupont, G. Marchal, and P. Suetens, "Reduction of metal streak artifacts in X-ray computed tomography using a transmission maximum a posteriori algorithm," *IEEE Trans. Nucl. Sci.*, vol. 47, no. 3, pp. 977–981, Mar. 2000.

[106] B. De Man, "Iterative reconstruction for reduction of metal artifacts in computed tomography," Dept. Elect. Eng., Univ. Leuven, Leuven, Belgium, Tech. Rep. ISBN 90-5682-300-0, 2001.

[107] N. Menvielle, "Reduction des artefacts metalliques en tomographie a rayons X," Inst. Biomed. Eng., Ecole Polytechnique de Montreal, Montreal, QC, Canada, 2004.

[108] B. De Man, J. Nuyts, P. Dupont, G. Marchal, and P. Suetens, "An iterative maximum-likelihood polychromatic algorithm for CT," *IEEE Trans. Med. Imag.*, vol. 20, no. 10, pp. 999–1008, Oct. 2001.

[109] B. Hamelin *et al.*, "Iterative CT reconstruction of real data with metal artifact reduction," in *Proc. IEEE Int. Symp. Biomed. Imag.*, May 2008, pp. 1453–1456.

[110] K. Van Slambrouck and J. Nuyts, "Metal artifact reduction in computed tomography using local models in an image block-iterative scheme," *Med. Phys.*, vol. 39, no. 11, p. 7080, 2012.

[111] M. Oehler and T. M. Buzug, "Statistical image reconstruction for inconsistent CT projection data," *Methods Inf. Med.*, vol. 46, no. 3, pp. 261–269, 2007.

[112] B. Kratz and T. Buzug, "Metal artifact reduction in computed tomography using nonequispaced Fourier transform," in *Proc. IEEE Nucl. Sci. Symp. Conf.*, Oct./Nov. 2009, pp. 2720–2723.

[113] S. Aootaphao, C. Pintavirooj, and S. Sotthivirat, "Penalized-likelihood reconstruction for metal artifact reduction in cone-beam CT," in *Proc. IEEE 30th Annu. Int. Conf. Eng. Med. Biol. Soc. (EMBS)*, Aug. 2008, pp. 2733–2736.
[114] X. Zhang, J. Wang, and L. Xing, "Metal artifact reduction in X-ray computed tomography (CT) by constrained optimization," *Med. Phys.*, vol. 38, no. 2, pp. 701–711, 2011.
[115] A. Kalvin and B. Williamson, "Using scout images to reduce metal artifacts in CT with application to revision total hip surgery," in *Proc. SPIE 3034, Med. Imag., Image Process.*, Apr. 1997, pp. 1017–1028.
[116] A. D. Kalvin, "System and method for reducing reconstruction artifacts in computed tomography images," U.S. Patent 5 933 471, Aug. 3, 1999.
[117] G.-H. Chen, J. Tang, and S. Leng, "Prior image constrained compressed sensing (PICCS): A method to accurately reconstruct dynamic CT images from highly undersampled projection data sets," *Med. Phys.*, vol. 35, no. 2, pp. 660–663, 2008.
[118] D. L. Snyder *et al.*, "Deblurring subject to nonnegativity constraints when known functions are present with application to object-constrained computerized tomography," *IEEE Trans. Med. Imag.*, vol. 20, no. 10, pp. 1009–1017, Oct. 2001.
[119] J. A. O'Sullivan and J. Benac, "Alternating minimization algorithms for transmission tomography," *IEEE Trans. Med. Imag.*, vol. 26, no. 3, pp. 283–297, Mar. 2007.
[120] R. J. Murphy *et al.*, "Pose estimation of known objects during transmission tomographic image reconstruction," *IEEE Trans. Med. Imag.*, vol. 25, no. 10, pp. 1392–1404, Oct. 2006.
[121] J. W. Stayman, Y. Otake, J. L. Prince, A. J. Khanna, and J. H. Siewerdsen, "Model-based tomographic reconstruction of objects containing known components," *IEEE Trans. Med. Imag.*, vol. 31, no. 10, pp. 1837–1848, Oct. 2012.
[122] G. Henrich, "A simple computational method for reducing streak artifacts in CT images," *Comput. Tomogr.*, vol. 4, no. 1, pp. 67–71, 1980.
[123] H. Soltanian-Zadeh, J. P. Windham, and J. Soltanianzadeh, "CT artifact correction: An image-processing approach," in *Proc. SPIE 2710, Med. Imag., Image Process.*, Apr. 1996, pp. 477–485.
[124] M. Bal, H. Celik, K. Subramanyan, K. Eck, and L. Spies, "A radial adaptive filter for metal artifact reduction," in *Proc. SPIE 5747, Med. Imag., Image Process.*, 2005, pp. 2075–2082.
[125] O. Watzke and W. A. Kalender, "A pragmatic approach to metal artifact reduction in CT: Merging of metal artifact reduced images," *Eur. Radiol.*, vol. 14, no. 5, pp. 849–856, 2004.
[126] E. Meyer, R. Raupach, M. Lell, B. Schmidt, and M. Kachelrieß, "Frequency split metal artifact reduction (FSMAR) in computed tomography," *Med. Phys.*, vol. 39, no. 4, p. 1904, 2012.
[127] A. Mouton, N. Megherbi, G. T. Flitton, S. Bizot, and T. P. Breckon, "A novel intensity limiting approach to Metal Artefact Reduction in 3D CT baggage imagery," in *Proc. Int. Conf. Image Process., (ICIP)*, 2012, pp. 2057–2060.
[128] H. Ballhausen, M. Reiner, U. Ganswindt, C. Belka, and M. Söhn, "Post-processing sets of tilted CT , vol. as, a method for metal artifact reduction," *Radiat. Oncol.*, vol. 9, no. 1, p. 114, 2014.
[129] J. Y. Huang *et al.*, "An evaluation of three commercially available metal artifact reduction methods for CT imaging," *Phys. Med. Biol.*, vol. 60, no. 3, p. 1047, 2015.
[130] M. Kidoh *et al.*, "Reduction of dental metallic artefacts in CT: Value of a newly developed algorithm for metal artefact reduction (O-MAR)," *Clin. Radiol.*, vol. 69, no. 1, pp. e11–e16, 2014.
[131] Y. Xi, Y. Jin, B. De Man, and G. Wang, "High-kVp assisted metal artifact reduction for X-ray computed tomography," *IEEE Access*, vol. 4, pp. 4769–4776, Aug. 2016.
[132] L. Liu, "Model-based iterative reconstruction: A promising algorithm for today's computed tomography imaging," *J. Med. Imag. Radiat. Sci.*, vol. 45, no. 2, pp. 131–136, 2014.
[133] S. Boudabbous, D. Arditi, E. Paulin, A. Syrogiannopoulou, C. Becker, and X. Montet, "Model-based iterative reconstruction (MBIR) for the reduction of metal artifacts on CT," *Amer. J. Roentgenol.*, vol. 205, no. 2, pp. 380–385, 2015.
[134] G. Delso, S. Wollenweber, A. Lonn, F. Wiesinger, and P. Veit-Haibach, "MR-driven metal artifact reduction in PET/CT," *Phys. Med. Biol.*, vol. 58, no. 7, p. 2267, 2013.
[135] A. K. Louis and A. Rieder, "Incomplete data problems in X-ray computerized tomography," *Numer. Math.*, vol. 56, no. 4, pp. 371–383, 1989.
[136] P. Maass, "The interior radon transform," *SIAM J. Appl. Math.*, vol. 52, no. 3, pp. 710–724, 1992.
[137] D. Silver *et al.*, "Mastering the game of Go with deep neural networks and tree search," *Nature*, vol. 529, no. 7587, pp. 484–489, Jan. 2016.

LARS GJESTEBY received the B.S. degree in biomedical engineering from the Rensselaer Polytechnic Institute, Troy, NY, USA, in 2014, where is currently pursuing the Ph.D. degree in biomedical engineering under the advisement of G. Wang. His research interests are x-ray computed tomography, metal artifact reduction, deep learning, and the combination of computed tomography and MRI for simultaneous imaging.

BRUNO DE MAN received the B.S., M.S., and Ph.D. degrees from Katholieke Universiteit Leuven, Leuven, Belgium, in 1995, 1995, and 2001, respectively, all in electrical engineering. He pioneered the use of statistical iterative reconstruction methods for computed tomography (CT), developed accurate CT simulation models, and studied new methods for metal artifact reduction. After he joined the General Electric Global Research (GEGR) Center, Niskayuna, NY, USA, in 2001, he continued his research in CT iterative reconstruction in collaboration with the University of Michigan, Ann Arbor, MI, USA, Purdue University, West Lafayette, IN, USA, and the University of Notre Dame, Notre Dame, IN, USA. This work led to the commercial introduction of Veo by GE Healthcare (GEHC) in 2010. He is known for the development of distance-driven projection, a technique that was adopted in both the CT and PET industry. He was one of the two original authors of CatSim, a CT simulation package widely used by GEGR Center and academic partners. He was a part of the team that developed the reconstruction algorithms used on the recent GEHC CT product scanners. In collaboration with Stanford University, Stanford, CA, USA, he and his team developed the first multi-source inverse-geometry CT scanner. He also has a long-term collaboration with the Rensselaer Polytechnic Institute, Troy, NY, USA (formerly with the Virginia Polytechnic Institute and State University, Blacksburg, VA, USA, and Wake Forest University, Winston-Salem, NC, USA) to develop novel cardiac CT architectures, with the University of Washington, Seattle, WA, USA, to develop ultralow-dose techniques for PET-CT attenuation correction and the Massachusetts General Hospital, Boston, MA, USA, to develop organ targeting and adaptive sequencing for sub-mSv imaging. He is currently the Manager of the CT Systems and Applications Laboratory and CT Research Portfolio Leader with GEGR Center. He holds 99 U.S. patent applications and has authored over 100 international publications.

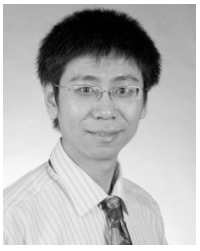

YANNAN JIN received the B.S. and M.S. degrees in biomedical engineering from Shanghai Jiao Tong University, Shanghai, China, in 2005 and 2008, respectively, and the Ph.D. degree in medical physics from the University of Erlangen-Nuremberg, Germany, in 2011, with a focus on the implementation and optimization of dual energy CT. His master's thesis was on the exact reconstruction of helical cone beam computed tomography (CT). He joined General Electric Global Research Center, Niskayuna, NY, USA, in 2011, where he was involved on the CT physics correction and calibration, dual energy CT, spectral imaging, and CT dose reduction with patient and application specific scanning protocol optimization. He is currently a Lead Engineer with the Image Reconstruction Laboratory, General Electric Global Research Center.

HARALD PAGANETTI received the Ph.D. degree in nuclear physics from Rheinische-Friedrich-Wilhelms University, Bonn, Germany, in 1992. He joined the Physics Team, Massachusetts General Hospital, in 1998, where he was involved in medical physics. He is currently the Director of Physics Research for Radiation Oncology with Massachusetts General Hospital and a Professor with the Harvard Medical School. He has authored or co-authored over 180 peer-reviewed publications and has edited two books on Proton Therapy. He has made significant contributions to the field of radiation oncology physics, many of which have found their way into clinical practice. Particularly, he is a pioneer in advanced Monte Carlo dose calculations for proton therapy treatment planning, which allowed the reduction of treatment planning margins for many patients, and in four-dimensional dose calculation aiming at a better understanding of motion effects when using radiation therapy for moving targets. He is considered the world Expert on the relative biological effectiveness of proton beams and has had a significant impact in biological effect modeling. For his research, he has been awarded numerous grants from the National Cancer Institute and the industry, which allows him to head a research laboratory of 25 researchers, the majority post-doctoral fellows, and students. In 2014, he received the Excellence in Mentoring Award from the Harvard Medical School. He serves on various committees mainly for the American Association of Physicists in Medicine, for which he was named Fellow in 2014, and American Society for Therapeutic Radiology and Oncology (ASTRO). Notably, he is the Chair of the Clinical, Translational, and Basic Science Advisory Committee of ASTRO as well as the Chair of the ASTRO physics track. He is a member of the National Council on Radiation Protection and Measurements.

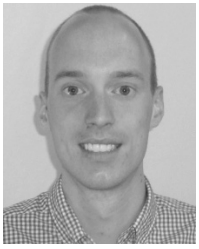

JOOST VERBURG received the B.Sc., M.Sc., and Ph.D. degrees from the Eindhoven University of Technology, The Netherlands, in 2009, 2011, and 2015, respectively, all in applied physics. He is currently a Research Fellow with the Department of Radiation Oncology, Massachusetts General Hospital and Harvard Medical School, Boston, MA, USA. He is also leading the development of a prototype system for the first clinical studies of this technology. His research focuses on the development of imaging technology to improve the clinical benefit of proton radiotherapy, by enhancing the accuracy of the radiation delivery. He has developed algorithms to reduce artifacts in computed tomography scans of patients with metallic implants and he has contributed to integrated infrastructure for the Monte Carlo simulation of clinical treatment plans. Recently, he developed a novel method for in vivo verification of proton beams, based on the spectroscopy of gamma rays from proton-nuclear interactions with the patient's tissue. For this work, he received young investigator awards at the American Association of Physicists in Medicine annual meeting and the IEEE medical imaging conference.

DROSOULA GIANTSOUDI received the Diploma degree in applied mathematical and physical sciences from the National Technical University of Athens, Greece, in 2005, and the Ph.D. degree in radiological sciences (medical physics) from the University of Texas Health Science Center at San Antonio, TX, USA, in 2011, with a focus on biologically based optimization of brachytherapy treatment techniques. Her Diploma thesis was on experimental nuclear physics and detector commissioning. Additional projects included Monte Carlo commissioning of radiation therapy equipment, studying the dosimetric effect of computed tomography image quality and daily patient setup uncertainties and developing in-house dosimetric software solutions for the clinic. She joined the Radiation Oncology Physics Research Group, Massachusetts General Hospital, Boston, MA, in 2011, where she was involved in proton radiation therapy. She has also involved in the dosimetric evaluation of analytical and fast GPU-based dose calculation algorithms, based on Monte Carlo dose calculation techniques. She is studying correlations between radiation therapy clinical outcomes and proton's relative biological effectiveness, and utilizes biologically related information as guidance in proton therapy treatment planning.

GE WANG (F'03) received the Ph.D. degree in electronics and communication engineering. He is currently the Clark & Crossan Endowed Chair Professor and the Director of Biomedical Imaging Center/Cluster, Rensselaer Polytechnic Institute, Troy, New York, USA. His expertise includes x-ray computed tomography (CT), optical molecular tomography, multi-modality imaging, and deep learning. He wrote the pioneering papers on the first spiral cone-beam CT algorithm (1991 and 1993). Spiral/helical cone-beam/multi-slice CT imaging is constantly used in almost all hospitals worldwide. There are over 85 million CT scans yearly in USA alone, with a majority in the spiral cone-beam/multi-slice mode. He and his collaborators published the first paper on bioluminescence tomography, creating a new area of optical molecular tomography. His group published the first papers on interior tomography and omni-tomography for grand fusion of all relevant tomographic modalities (all-in-one) to acquire different datasets simultaneously (all-at-once) with simultaneous CT-MRI as an example. His results were featured in Nature, Science, and PNAS, and recognized with various academic awards. He authored over 400 journal papers, which are highly cited. His group has been in close collaboration with world-class groups, and continuously well funded by federal agents. He is a fellow of SPIE, OSA, AIMBE, AAPM, and AAAS. He is the Lead Guest Editor of four IEEE TRANSACTIONS on MEDICAL IMAGING special issues on x-ray CT, the *Molecular Imaging*, the *Compressive Sensing, and the Spectral CT*, the founding Editor-in-Chief of the *International Journal of Biomedical Imaging*, and an Associate Editor of the IEEE Transactions on MEDICAL IMAGING and the *Medical Physics*.